AD-A133 809 FRACTURE TOUGHNESS OF FIBER REINFORCED CONCRETE(U) 1/
NORTHWESTERN UNIV EVANSTON IL DEPT OF CIVIL ENGINEERING
M WECHARATANA ET AL. 01 JUN 83 AFOSR-TR-83-0876
UNCLASSIFIED AFOSR-82-0243 F/G 11/2 NL

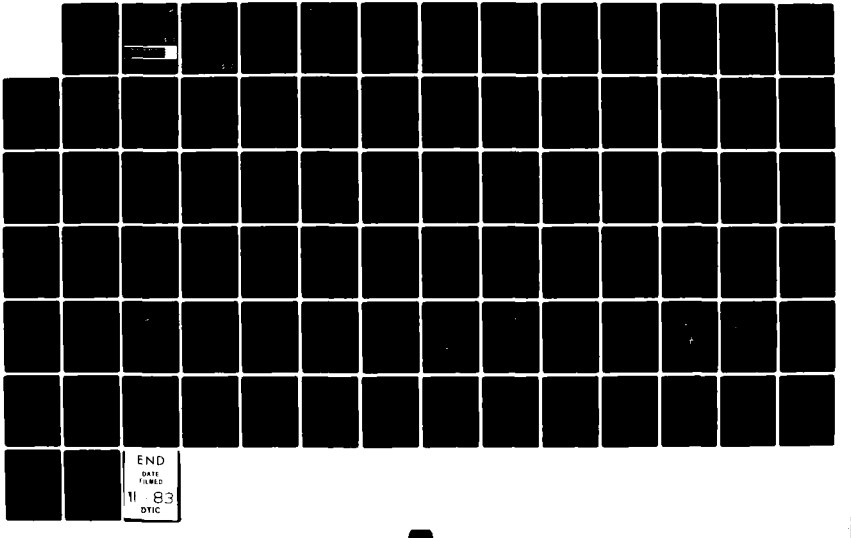

END
DATE FILMED
11-83
DTIC

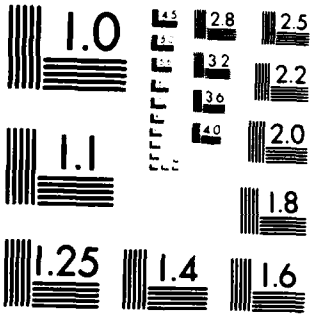

AFOSR-TR- 83-0876

Technological Institute
NORTHWESTERN UNIVERSITY
EVANSTON, ILLINOIS

Approved for Public Release; Distribution Unlimited

12

A Progress Report on Fracture Toughness of Fiber Reinforced Concrete

AFOSR-820243
Principal Investigator: S.P. Shah

Prepared by

M. Wecharatana* and S. P. Shah

Department of Civil Engineering

Northwestern University

June 1983

---

* Now at New Jersey Institute of Technology

Unclassified

SECURITY CLASSIFICATION OF THIS PAGE (When Data Entered)

REPORT DOCUMENTATION PAGE	READ INSTRUCTIONS BEFORE COMPLETING FORM
1. REPORT NUMBER AFOSR-TR- 83-0876 2. GOVT ACCESSION NO.	3. RECIPIENT'S CATALOG NUMBER
4. TITLE (and Subtitle) Fracture Toughness of Fiber Reinforced Concrete	5. TYPE OF REPORT & PERIOD COVERED Progress Report June 1982 - June 1983
	6. PERFORMING ORG. REPORT NUMBER
7. AUTHOR(s) M. Wecharatana and S.P. Shah	8. CONTRACT OR GRANT NUMBER(s) AFOSR - 82 - 0243
9. PERFORMING ORGANIZATION NAME AND ADDRESS Department of Civil Engineering Northwestern University Evanston, Illinois 60201	10. PROGRAM ELEMENT, PROJECT, TASK AREA & WORK UNIT NUMBERS 2307/C2 61102F
11. CONTROLLING OFFICE NAME AND ADDRESS Air Force Office of Scientific Research Bolling AFB, DC 20332	12. REPORT DATE June 1, 1983
	13. NUMBER OF PAGES 71
14. MONITORING AGENCY NAME & ADDRESS(if different from Controlling Office)	15. SECURITY CLASS. (of this report) Unclassified
	15a. DECLASSIFICATION/DOWNGRADING SCHEDULE

16. DISTRIBUTION STATEMENT (of this Report)

Approved for public release, distribution unlimited

17. DISTRIBUTION STATEMENT (of the abstract entered in Block 20, if different from Report)

18. SUPPLEMENTARY NOTES

Part of this report will be published in Cement and Concrete Research

19. KEY WORDS (Continue on reverse side if necessary and identify by block number)

blast resistant protective concrete structures, fracture mechanics, reinforced concrete, cracking resistance, steel fibers, post-peak response, pull-out vs. slip relationship

20. ABSTRACT (Continue on reverse side if necessary and identify by block number)

For fiber reinforced cement based composites, the principal beneficial effects of fibers (metallic, mineral or organic) accrue after the matrix has cracked. For loads beyond which the matrix has initially cracked, the further crack extension and opening is resisted by bridging of fibers across the cracks. The resistance provided by the fibers will depend principally on the debonding and the pull-out resistance of fibers. (over)

DD FORM 1 JAN 73 1473 EDITION OF 1 NOV 65 IS OBSOLETE

Unclassified

SECURITY CLASSIFICATION OF THIS PAGE (When Data Entered)

20. (con't)

A theoretical model based on the concepts of nonlinear fracture mechanics to predict the resistance provided by the fibers against the fracture of matrix is presented in this report. The theoretically predicted response is compared favorably with the experimental data on notched beams and double cantilever beam specimens of steel fiber reinforced concrete. The proposed theoretical model provides a method to calculate fracture reisitance for a crack extension in a specimen of any geometry.

One of the key parameters required for the model is the relationship between the uniaxial post-cracking stress and the corresponding displacement. This relationship will depend on the bond-slip function of fibers. A method to estimate this relationship is presented.

TABLE OF CONTENTS

ABSTRACT

For fiber reinforced cement based composites, the principal beneficial effects of fibers (metallic, mineral or organic) accrue after the matrix has cracked. For loads beyond which the matrix has initially cracked, the further crack extension and opening is resisted by bridging of fibers across the cracks. The resistance provided by the fibers will depend principally on the debonding and the pull-out resistance of fibers.

A theoretical model based on the concepts of nonlinear fracture mechanics to predict the resistance provided by the fibers against the fracture of matrix is presented in this report. The theoretically predicted response is compared favorably with the experimental data on notched beams and double cantilever beam specimens of steel fiber reinforced concrete. The proposed theoretical model provides a method to calculate fracture resistance for a crack extension in a specimen of any geometry.

One of the key parameters required for the model is the relationship between the uniaxial post-cracking stress and the corresponding displacement. This relationship will depend on the bond-slip function of fibers. A method to estimate this relationship is presented.

INTRODUCTION AND SUMMARY OF CONCLUSIONS

Research conducted during the last twenty years has shown that the addition of fibers significantly improves penetration, scabbing and fragmentation resistance of concrete. The possible applications of fiber reinforced concrete (FRC) include explosion and shock resistant protective structures. Even though the enhanced "cracking resistance" is the most important attribute of FRC, there are no rational methods of measuring or predicting this important materialproperty.

For fiber reinforced cement based composites, the pricipal beneficial effects of fibers (metallic, mineral or organic) accrue after the cracking of matrix has occured. For loads beyond which the matrix has initially cracked, the further crack extension and opening is resisted by bridging of fibers across the crack. To incorporate the effects of fibers bridging, many investigators have used the classical linear elastic fracture mechanics concepts. These past attempts however assume one or more of the following: (1) the closing pressure due to the fiber-bridging is constant, (2) the extent of the fiber bridging zone is small compared to the length of the traction free crack length, and (3) ignore the energy absorbed in the fiber-bridging zone. In this report the results of a theoretical model which does not make the above assumptions are presented.

An existing crack in a cement based matrix is replaced by an effective crack length which consists of three zone: (1) a traction free zone, (2) fiber bridging zone (ℓ_f), and (3) the matrix process zone (ℓ_p) resulting from the aggregate interlock and microcracking (Fig. 5). It is assumed that the stresses and deformations due to the applied loads and

the closing pressures can be calculated using theory of elasticity. The fiber bridging closing pressure depends on the crack opening displacement which in turn depends on the geometry of the specimen, external loading and on the closing pressure itself. An iterative procedure was developed to account for this coupling between the closing pressure and the crack opening displacement.

Experiments with fiber reinforced concrete specimens subjected to uniaxial tension in a relatively stiff testing system indicate that the post-peak displacement are essentially a result of opening of a single crack. Thus it was assumed that the relationship between fiber bridging closing pressure and the crack opening displacement (COD) are equivalent to the uniaxial, tensile, post-peak stress-displacement function. A method to estimate this relationship is proposed (Fig. 8) for steel fiber reinforced concrete. Experiments to verify this concept are currently underway at Northwestern University. Based on these experiments it is expected to derive closing pressure vs. crack opening displacement relationship from a single fiber pull-out vs. slip function.

Based on the theoretical model, load vs. crack mouth displacement curves for notched, steel-fiber reinforced concrete beams were derived and compared with experimental data (Fig. 26). The crack opening displacements for the theoretical model were calculated using some simple approximations. A more rigorous method of calculating COD by modelling crack as distributed dislocations is currently underway.

Fracture resistance vs. crack extension relationships (R-curves) were calculated and compared with the experimental data on the double cantilever

beam specimens of steel FRC (Fig. 20). The theoretical curves were obtained by assuming that the displacement resulting from the fiber bridging forces are irreversible. A good correlation was obtained with the experimentally observed R-curves as well as load vs. load-line displacement curves (Fig.22). Note that if the asymptotic value of R-curves is considered a material parameter, then that value can be a useful quantity in identifying the benefits of fiber addition. For example the predicted steady state value for specimens reinforced with 37.5 mm steel fibers is approximately 40 times that for plain unreinforced matrix (Fig. 25). This relative improvement in fracture energy is comparable to that obtained by using an empirical method called toughness index suggested by American Concrete Institute.

PREVIOUS THEORETICAL MODELS

Many investigators have attempted to predict the fracture behavior of fiber reinforced composites based on the fiber bridging concept [2, 3, 4, 12, 13].

Lenian and Bunsell [2] proposed that the stress intensity factor (K_R) required for crack propagation was the algebraic sum of the stress intensity factors resulting from the external load applied to the cracked specimen and without considering the presence of fibers (K_o) and the stress intensity factor due to fibers bridging across the crack (K_r), i.e.,

$$K_R = K_o - K_r = K_c \tag{1}$$

where K_c = experimentally determined critical stress intensity factor for the unreinforced matrix.

They calculated the effect of fibers bridging (K_r) in Asbestos Cement by employing Paris and Sih's analytical expression [14] which was derived for an internal crack in an infinite sheet under a region of uniform closing pressure σ applied at the crack tip (Fig. 1-a). This relationship is given as:

$$K_r = \sigma\frac{\sqrt{a}}{\sqrt{\pi}}\left[\sin^{-1}\frac{c}{a} - \sin^{-1}\frac{b}{a} - (1 - \frac{c^2}{a^2})^{\frac{1}{2}} + (1 - \frac{b^2}{a^2})^{\frac{1}{2}}\right] \tag{2}$$

where a, b, and c are crack length, and the boundaries of the applied uniform pressure σ, as shown in Fig. 1-a.

They assumed that the closing stresses produced by the asbestos fibers were the same for microcracks as for the main crack, and that a zone of microcracking of length ℓ_p can be represented by an imaginary increase of crack length, $x\ell_p$, where x is a factor less than unity, to which the closing stress was uniformly applied (Fig. 1-b).

The stress intensity factor (K_R) was then calculated as:

$$K_R = K_o - \frac{\sigma}{\sqrt{\pi}}(a + x\ell_p)^{\frac{1}{2}} \left(\frac{\pi}{2} - \sin^{-1} \frac{a_o}{(a + x\ell_p)} + \left[1 + \frac{a_o^2}{(a + x\ell_p)^2} \right]^{\frac{1}{2}} \right) \quad (3)$$

where x was the fraction of the microcracked zone ℓ_p. Note that σ is the uniform bridging pressure of asbestos fibers which was assumed equal to the maximum value of the post-cracking stress (σ_{max}) and was calculated from [15]:

$$\sigma_{max} = A_1 V_m \sigma_m + 4 \eta_\ell \eta_\theta \tau V_f \frac{\ell}{d} \quad (4\text{-a})$$

Where A_1 is a factor related to the extent of matrix cracking and which is equal to or less than unity, V_m and σ_m are the percent volume fraction of the matrix and the matrix tensile strength. The second term in Eq. (4-a) is primarily the contribution from fibers being pulled out. η_ℓ is the efficiency factor for the embedment length of fibers. η_θ is the coefficient for fiber orientation and distribution, while τ, V_f, and $\frac{\ell}{d}$ are the bond strength of fiber-matrix interface, fiber volume fraction, and the aspect ratio, respectively.

The matrix-cracking factor A_1 is usually small and can normally be neglected (equals zero). The values of η_ℓ, η_θ and τ are generally a function of specimen geometrics, casting procedure, type and size of fibers, fiber volume fraction, and fiber distribution (1-D, 2-D, or 3-D).

By introducing $A_2 = 4 \eta_\ell \eta_\theta \tau$, Eq. (4-a) can be rewritten as:

$$\sigma_{max} = A_1 V_m \sigma_m + A_2 V_f \frac{\ell}{d} \quad (4\text{-b})$$

The values of A_1 and A_2 are varied depending on different testing configurations, conditions of matrix cracking and fiber debonding. In this study, the value of A_1 was assumed to be zero while different values of A_2 were selected, depending from different testing and cracking conditions.

Their theoretical model did not provide good correlation with the experiment results. This may be explained from the fact that, firstly, they used a solution which was derived for a crack in an infinite sheet to represent a specimen with finite boundaries. Secondly, the actual fiber bridging pressure depends on the crack surface displacement. This implies that the assumption of constant fiber bridging pressure is not an accurate one. Thirdly, their method of including the effect of the matrix process zone by a factor x may not be very accurate because x reduces the effective crack length which influences K_o and K_r.

Foote, Cotterell and Mai [3] proposed a model using the LEFM analyses for a semi-infinite crack (Fig. 2). They also assumed that the stress intensity factor (K_R) for propagating a crack in fiber reinforced concrete specimen consisted of two components, i.e.,

$$K_R = K_o - K_r \tag{5}$$

where K_o is the stress intensity factor at the tip of the crack if there were no fibers bridging and K_r is the stress intensity factor due to the bridging fibers which tends to close the crack and was therefore considered as negative (this is similar to Lenian and Bunsell's model [2]).

However, they realized that the fiber bridging stresses (crack closing stresses) were coupled to the crack-surface displacements which in turn was a function of the external loading and the crack closing stresses. To solve this problem, they assumed a fifth order polynomial for the crack closing stress, $\sigma(t)$. By employing the semi-infinite crack concept and the analytical expression from Muskhelishvili's potential function [16] which gives the displacements of the crack faces due to closing pressure $\sigma(t)$, they

calculated the displacement and stress intensity factor due to fiber bridging as:

$$\Phi(Z) = \frac{1}{2\pi i\sqrt{Z}} \int_0^\infty \frac{\sigma(t)\sqrt{t}}{(t - Z)}\, dt \tag{6}$$

$$u_r = \frac{4}{E} I_m \int_0^Z \Phi(Z)\, dZ \tag{7}$$

$$K_r = -\left[\frac{2}{\pi}\right]^{\frac{1}{2}} \int_0^\infty \frac{\sigma(t)}{\sqrt{t}}\, dt \tag{8}$$

where u_r and K_r are the displacement and the stress intensity factor due to the bridging fibers.

The displacement for the crack without fiber bridging (u_o) was determined from theory of elasticity as:

$$u_o = \frac{2 K_o}{E}\sqrt{\frac{2t}{\pi}} \tag{9}$$

where Poissons' ratio ν was neglected in Eq. (9), ($\nu = o$).

With the calculated total displacement, $u = u_o + u_r$, an iterative method was adopted to determine the K_R curve for asbestos-cement composite, using the initiation criterion as K_R equalled K_c (a critical initiation value for matrix) :

$$K_R = K_o + K_r = K_c \tag{10}$$

The comparison of the predicted results with the experimental values was poor. They attributed it to the fact that the assumed crack closing pressure was inaccurate due to lack of experimental data. Besides, the semi-infinite crack solution was clearly not the actual solution for a finite specimen and crack growth.

Since the crack closing stress $\sigma(t)$ on the crack surfaces depends on the displacement, u(r), and in turn the displacement u(r) depends on the stress function $\Phi(Z)$, Eq. (6) cannot be solved directly without knowing the exact $\sigma(t)$ and therefore an iterative method is used. By assuming a fifth order polynomial function as the initial value of $\sigma(t)$, u(r) was then calculated from Eqs. 6 and 7, and the crack closing stress $\sigma(t)$ was determined and iterated.

Using two types of test specimens, double cantilever beam and single edge notched, Bowling and Groves [4] explained that as the crack propagated in the DCB specimen and became bridged by the aligned nickel wires (Fig. 3), the measured critical stress intensity factor, for further propagation, increased.

The increase was clearly due to the presence of wires bridging the crack and exerting crack closing pressure which reduced the actual stress intensity factor pertaining to the matrix crack tip. Thus a stress intensity factor due to wires bridging (K_w) must be subtracted from that due to the applied force (K_a) and the initiation criterion was set as the net stress intensity factor ($K_a - K_w$) reached the critical value of K_{IC}, i.e.,

$$K_a - K_w = K_{IC} \tag{11}$$

The K_{IC} value here was taken as that required for propagating an unbridged crack past a wire. The value of K_a for the case of DCB was calculated from an expression given by Wiederhorn et al [17] as:

$$K_a = \frac{Pa}{w^{1/2}b^{1/2}d^{3/2}} \left(3.457 + 2.315 \frac{d}{a} \right) \tag{12}$$

where P was the applied load, a was the measured crack growth, and w, b, and d were specimen dimensions as defined in Fig. 3.

To calculate the contribution of the bridging wire (K_w), P in Eq. (12) was substituted by the tensile force in the wire, and a was replaced by the distance from the wire to the crack tip.

The main argument for this proposed model was that the assumed crack bridging force P was independent of crack opening displacement which is unlikely to be the case of fiber reinforced concrete [3, 12, 13, 19, 20, 21]. The effect of matrix process zone in front of the crack tip was also neglected. The analysis was primarily designed for the aligned fibers and therefore cannot be used for the case of random distributed fibers. The formula given in Eq. (12) was also based on the elastic analysis which is unlikely to be applicable, without any modification, to nonlinear materials such as concrete and fiber reinforced composites.

Petersson and Hillerborg [12, 13] introduced a fictitious crack model using finite element analysis to determine fracture toughness of concrete and fiber reinforced composites. Their model was based on the Dugdale-Barenblatt concept [10, 18] which primarily depends on the stress- displacement relationship in the nonlinear zone (fiber bridging and matrix process zone). Their stress-displacement relationship (σ vs η) can either be obtained from a uniaxial tensile test or from a notched beam specimen. A set of linear stress-displacement relationships was assumed in the analysis. By keeping the work done or area under the $\sigma - \eta$ curve constant, the maximum pulled-out displacement (η_f^{max}) which was later used as the initiation criterion (Fig. 4) was calculated from:

$$G_c = \int_0^{\eta_f^{max}} \sigma \, d(\eta) \qquad (13)$$

With the linear $\sigma - \eta$ relationship, the maximum pulled-out displacement η_f^{max} can be expressed as:

$$\eta_f^{max} = \frac{2G_c}{\sigma_{max}} \tag{14}$$

It can be seen that the value of η_f^{max} was calculated as a function of only G_c and $(\sigma_c)_{max}$. However, η_f^{max} should be primarily a function of fiber geometry and distribution. For example, it is shown that the upperbound value of η_f^{max} equals $\frac{\ell}{2}$ whether fibers are steel or glass even though the values of G_f/σ_{max} may be different for these two types of fibers.

BASIC CONCEPTS OF THE PROPOSED MODEL

A crack just prior to its extension in Mode I opening in a fiber reinforced concrete specimen is shown in Fig. 5. The length of the crack can be divided into three regions: 1) a traction-free crack length which consists of initial cast notch and the zone of crack length where fibers are completely pulled out of the matrix, 2) the region of fiber bridging (ℓ_f), and 3) the matrix process zone (generally due to aggregate debonding and interlocking) in front of the crack tip. Both fiber bridging and matrix process zone provide resistance to crack opening. The effect of the fiber bridging is normally much more significant than that contributed from the matrix process zone, and as a result, the crack closing pressure in the matrix process zone is neglected in this study.

Region 1 (traction-free crack) and region 2 (fiber bridging) were separated at the point where the crack surface displacement was equal to η^f_{max} (the maximum crack displacement where fiber bridging stress is zero, since all fibers at that point are completely pulled out, Fig. 6), while the fiber bridging zone and the matrix process zone were divided at the point where crack surface displacement equalled to η^m_{max} (the maximum displacement of the matrix in the descending branch of the uniaxial tensile test where stress is equal to zero, Fig. 6).

The value of η^m_{max} has been reported by Wecharatana and Shah [19, 20, 21]. This value is about 0.8×10^{-3} in. for matrix mix 1:2:0:0.5 (c:6:A:w). The η^f_{max} value used in this study was half the fiber length. This may be justified (as shown in Fig. 6) from the observation that fibers are randomly distributed across the crack. The smallest pulled-out distance is equal to zero (labelled 3 in Fig. 6) and the largest pulled-out distance is half the

fiber length (labelled 2 in Fig. 6). This implies that if the two crack surfaces are separated by a distance of half the fiber length, there will not be any fibers left bridging across the crack which subsequently means the fiber bridging pressure is zero.

If fibers are randomly distributed rather than aligned, then the maximum embedment length approaches $\ell/2$ in. Similarly, the η^{m}_{max} refers to the crack surface displacement where zero aggregate bridging and interlocking pressure is assumed (Fig. 6).

If the stresses in these nonlinear zones (fiber bridging and matrix process zone) are assumed to be purely under uniaxial tensile behavior, then crack length "a" can be replaced by an effective (elastic) crack "a_{eff}" such that $a_{eff} = a + \ell_p$, where ℓ_p is the idealized length of the matrix process zone (Fig. 5). This effective crack "a_{eff}" sustains two types of crack closing pressures: one due to the fiber bridging and another due to aggregate bridging which was neglected as explained earlier. The concept of this model is somewhat similar to that originally proposed by Dugdale [10] and Barenblatt [18].

For a given applied load and an effective crack length, the crack opening process is primarily resisted by the bridging of fibers across the crack. It is necessary to first calculate the size of the fiber bridging zone. Since it is a function of the crack profile and the length of the fibers used, an approximate crack profile was first assumed (a linear crack profile was assumed in this study). Knowing the crack profile, crack length and η^{f}_{max} (half the fiber length), the size of fiber bridging zone was then determined. From the uniaxial tensile stress-displacement relationship and the assumed crack profile, the fiber bridging pressure can also be obtained.

The stress displacement relationships for different fiber volume fraction and aspect ratio are given in Table 1. Details of how to obtain such relationships will be discussed later.

In this analysis, it is assumed that crack will initiate as the crack surface displacement at the tip of the effective crack length "a" reaches a value η^{m}_{max} (defined in Figures 5 and 6).

As the fiber bridging pressure distribution depends on the crack surface displacement, which in turn is a function of the applied load, specimen geometry, the size of fiber bridging zone, the length of the matrix process zone ℓ_p and the closing pressure itself, an iterative procedure was then needed in the analysis as follows:

Consider a given crack length "a" in a fiber reinforced concrete specimen just prior to its further extension.

1. Assume a crack profile and a matrix process zone of length ℓ_p. With the given length of fibers used, the size of fiber bridging zone ℓ_f can be calculated using η^{f}_{max} as the limit of the fiber bridging zone.
2. Knowing ℓ_f and the assumed crack profile, calculate the closing pressure distribution, using the stress-displacement relationship given in Table 1. Note that for simplicity the closing pressure distribution in the matrix process zone is neglected.
3. For a given specimen geometry (double cantilever beam and notched beam specimens were considered here), the applied load P and the crack closing pressure, calculate, using theory of elasticity, the crack opening displacements for the effective crack a_{eff}.

4. If the crack opening displacement at the end of matrix process zone (ℓ_p) is equal to η^m_{max}, then the initiation criterion is satisfied and the assumed value of ℓ_p is partially a correct one; otherwise a new value of ℓ_p is assumed and the above steps are repeated until the initiation condition is satisfied.
5. To further ensure that the iterated ℓ_p and the assumed crack profile are correct, the load line deformation (η_p) is calculated based on the same elastic principle and then compared with the experimentally observed values. If these values do not correspond to the measured data, a new crack profile is assumed and the above procedure is repeated until this condition is satisfied.

NORMALIZED UNIAXIAL TENSILE STRESS-DISPLACEMENT RELATIONSHIP

Experiments with fiber reinforced concrete specimens subjected to uniaxial tension in a rigid testing system have shown that the post-peak displacements of the specimens are essentially a result of the opening of a single crack [22]. Thus the uniaxial tensile stress-displacement relationship in the post cracking region can be taken as the crack closing pressure (σ) versus crack surface displacement (η) relationship.

Since the uniaxial tensile stress-displacement is important to the fracture behavior of fiber reinforced concrete, careful study of this relation is essential, particularly in the post cracking region. Many investigations have conducted uniaxial tensile tests of fiber reinforced concrete with different fiber volume fractions and aspect ratios [12, 22, 23]. These results were used for the analysis here.

The stress-displacement relationship of fiber reinforced composites in the post-cracking region is bounded by two parameters (Fig. 7): the maximum post-cracking strength (σ_{max}) and the maximum pulled-out displacement of fiber (η^{f}_{max}).

The maximum post-cracking strength is generally known to be a function of fiber volume fraction (V_f), aspect ratio ($\frac{\ell}{d}$), fiber distribution and embedment length coefficient (β or 4 η_ℓ η_θ in Eq. 4-a) and the bond strength of fiber matrix interface (τ) [15] where:

$$\sigma_{max} = \beta \tau V_f \frac{\ell}{d} \tag{15}$$

The maximum fiber pulled-out displacement normally depends on the embedment length and the fibers orientation. It can be seen (Fig. 6) that fibers may bridge over a crack in different ways; some fibers may have most of the length embedded on one side, and have only a small portion left on the other side of the crack (labelled 1); some fibers may be totally embedded on one side of the crack (labelled 3); and hardly but possibly that a fiber may be equally embedded on both sides of the crack (labelled 2 in Fig. 6). Since the smaller side of the embedment length is the one which will be pulled out of the matrix (this is due to a smaller total resisting force or frictional force), it can then be concluded that the maximum pulled-out displacement cannot exceed half the fiber length which is used here as the value of η^{f}_{max} .

By normalizing the post-cracking stress with the maximum post-cracking strength (σ / σ_{max}) and the post-cracking displacement with η^{f}_{max}, ($\frac{\eta}{\eta^{f}_{max}}$), it was found that there exists a unique relationship between the normalized post-cracking stress and displacement for a given type of fiber.

This relationship was independent of the fiber volume fraction and aspect ratio as can be seen in Fig. 8. To generalize a unique normalized stress-displacement relationship for steel fiber reinforced concrete, it was assumed that the maximum post-cracking strength occurs at the end of the matrix process zone or the beginning of the fiber bridging zone, and smoothly decreases to zero as the crack-surfaces displacement reaches half of the fiber length. Therefore, the boundaries for this relationship can be summarized as:

$$\begin{aligned} &\text{at} \quad x = o \quad \text{or} \quad \eta = o \quad : \quad \frac{\sigma}{\sigma_{max}} = 1.0 \\ &\text{at} \quad x = \ell_f \quad \text{or} \quad \eta = \eta^f_{max} \quad : \quad \frac{\sigma}{\sigma_{max}} = 0.0 \end{aligned} \tag{16}$$

where x is the distance from the crack tip, η is the crack surface displacement at x. For the condition of monotorically decreasing stress, we can write:

$$\frac{d\sigma}{d\eta} < o \quad \text{for} \quad o < \eta < \eta^f_{max} \quad \text{or} \quad o < x < \ell_f \tag{17}$$

At attempt to predict the normalized stress-displacement relationships for steel fiber reinforced concrete based on the experimental results reported in [11, 22, 23] is made here. To satisfy all the required boundary conditions given in Eqs. (16, 17), one of the possible solutions is:

$$\frac{\sigma}{\sigma_{max}} = \left[1 - \frac{\eta}{\eta^f_{max}} \right]^2 \tag{18}$$

where σ_{max} is the maximum post-cracking strength and η^f_{max} is the maximum pulled-out displacement of fibers.

For other types of fiber reinforced composites, the normalized stress-displacement relationship given in Eq. 18 may be modified with an exponential factor of $e^{-A\left[\frac{\eta}{\eta^f_{max}}\right]^B}$ where Eq. 18 can be rewritten as:

$$\frac{\sigma}{\sigma_{max}} = \left[1 - \frac{\eta}{\eta^f_{max}}\right]^2 e^{-m\left\{\frac{\eta}{\eta^f_{max}}\right\}^n} \qquad (19)$$

where m and n are constants which will depend on the type and the pull-out behavior of fibers.

It can be seen that the post-cracking strength at any pulled-out displacement (η) can be predicted provided that η_{max} and η^f_{max} are known (σ_{max} is a function of η_ℓ , η_θ , τ , V_f, and ℓ/d while η^f_{max} equals half the fiber length). Thus the normalized relationship shown in Eqs. 8, 18, 19 could be very useful in design of fiber reinforced concrete composites.

To predict the tensile stress-displacement relationships in this study, the value of A_1 in Eq. 4-b was neglected and the factor A_2 which is a function of η_ℓ , η_θ , and τ has been selected from the literatures [15, 24 - 26] as follows:

For the double cantilever beam specimen, with the method of casting, the type of fibers used and the critical specimen thickness of 0.5 in. [11], the value of A_2 was selected as 600 psi. In the case of the notched beam specimens, the different fibers size, the method of casting, and specimen thickness of 1.5 in. [6], lead to the value of A_2 as 300 psi. With these selected values of A_2, the stress-displacement relationship can be predicted, using Eqs. 15 and 18.

Different $\sigma - \eta$ relationships for different fiber volume fraction and aspect ratio used in this study are given in Table 1.

CALCULATION OF CRACK SURFACE DISPLACEMENT

Most fracture studies for cementitious composites in the past were based on the calculation of the stress intensity factor K using the linear elastic fracture mechanics concept. In this study, a method is proposed to calculate the strain energy release rate G based on the change of global compliance $\frac{dC}{da}$ approach.

Approximate and simple methods of calculating compliances of a cracked double cantilever beam and centrally notched beam are described in the following section.

DOUBLE CANTILEVER BEAMS

The compliance of the double cantilever beam specimens was calculated using the so-called DCB approach [19, 20].

A single cantilever beam model under the applied load P and the crack closing pressure is shown in Fig. 9. The deformation for the double cantilever beam in this analysis was calculated from the beam bending theory where deformation due to the applied point-load P for a single cantilever beam (Fig. 9) can be determined from [19]:

$$y_p(x) = \frac{12P}{BE}\left[\frac{a_{eff}x^2}{2H(x)H^2(o)} - \frac{1}{C_2^3}\ln\frac{H(x)}{H(o)} - \frac{1}{2}\,\frac{x}{2}\left\{\frac{1}{H(x)} + \frac{1}{H(o)}\right\} + \frac{(1+\nu)}{4}\,\frac{1}{C_2}\ln\frac{H(o)}{H(x)}\right] \quad ; \quad C_2 = 0 \tag{20}$$

where $y_p(x)$ is the deformation at any point x from the effective crack tip,

a_{eff}. C_1 and C_2 are the beam depths at the free end and the slope of the tapered beam. E and υ are material constants, and B, H(x) and H(0) are beam width and thicknesses at distance x from crack tip and at the crack tip. These variables are shown in Fig. 9.

For the deformation due to fiber bridging pressure, with the nonlinear crack closing pressure, a numerical integration was employed to solve the beam bending governing equation:

$$\frac{d^2y}{dx^2} = \frac{M}{EI} + \frac{k}{AG}\frac{dV}{dx} \tag{21}$$

where A and I are cross sectional area and moment of inertia, E and G are elastic and shear modulus while K is the average shear constant. M and V are moment and shear which are given as:

for $\ell_p < x < \ell_f + \ell_p$;

$$M(x) = \int_x^{\ell_f + \ell_p} t_n \cdot \sigma(t)\,(t-x)\,dt$$

$$V(x) = \int_x^{\ell_f + \ell_p} t_n \cdot \sigma(t)\,dt \tag{22}$$

for $o < x < \ell_p$;

$$M(x) = \int_{\ell_p}^{\ell_f + \ell_p} t_n \cdot \sigma(t)\,(t-x)\,dt$$

$$V(x) = \int_{\ell_p}^{\ell_f + \ell_p} t_n \cdot \sigma(t)\,dt \tag{23}$$

for $x > \ell_f + \ell_p$;

$$M(x) = 0 \quad ; \quad V(x) = 0 \tag{24}$$

The total deformation is equivalent to the deformation due to applied load P subtracted by those due to fiber bridging.

$$(\eta_p)_{total} = (\eta_p)_{applied\ load} - (\eta_p)_{fiber\ bridging} \tag{25}$$

Details of the test setup and specimen dimensions are given in Fig. 10.

CALCULATION OF CRACK MOUTH DISPLACEMENT FOR NB SPECIMENS

A fiber reinforced concrete beam with an initial cast notch of length, a_o, subjected to pure bending, is shown in Fig. 11. As similar to the case of double cantilever beam analysis for a given load P and crack length "a", all nonlinear zones (matrix process zone and fiber bridging zone) were replaced by a region of crack closing pressure. The crack closing pressure within the matrix process zone was assumed to be small compared to those due to fiber bridging and therefore was neglected.

The fiber bridging stress again depends on the assumed crack profile which is a function of crack growth "a" and crack mouth displacement "CMD". Using the normalized stress-displacement relationship given in Eq. 18, the calculated maximum post-cracking strength (σ_{max}) and the assumed crack profile, the fiber bridging stress distribution can then be determined as follows:

For the assumed linear crack profile:

$$\frac{CMD}{a} = \frac{\eta}{y} \tag{26}$$

and

$$\eta = \frac{CMD}{a} \cdot y$$

Note that Eq. 26 gives $\eta = 0$ when $y = 0$ which is in fact not true. Only for the simplicity in calculating the fiber bridging pressure, this assumption is made.

Substitute η from Eq. 26 into the normalized stress-displacement relationship (Eq. 19). Eq. 18 can be rewritten as:

$$\sigma(y) = \sigma_{max} \left[1 - \frac{1}{\eta^{f}_{max}} \left(\frac{CMD}{a}\right) y \right]^2 \qquad (27)$$

where η^{f}_{max} is the maximum pulled-out displacement (equal to half the fiber length).

By introducing $A_k = \left(\frac{CMD}{a \cdot \eta^{f}_{max}}\right)$, Eq. 27 can be rewritten as:

$$\sigma(y) = \sigma_{max} \left[1 - A_k y \right]^2 \qquad (28)$$

Knowing the fiber bridging stress acting along the length of ℓ_f on the effective crack of length $a + \ell_p$, the change in rotation of the beam resulting from the effective crack - a_{eff} can be calculated from the relations derived by Okamura et al [27, 28]:

$$\theta = \lambda_{FM} \cdot F + \lambda_M \cdot M \qquad (29)$$

where θ is the relative rotation of the crack front, F is the axial force resulted from the fiber bridging pressure, M is the resultant moment due to the external load and those resisting moment due to F (Fig. 11), and λ_{FM} and λ_M are the increments of the compliances caused by the presence of the effective crack - a_{eff} and are given as:

$$\lambda_{FM} = \frac{2(1-\nu^2)}{BE} \frac{6}{W} \int_0^{\xi} \xi \, Y_F(\xi) \, Y_M(\xi) \, d\xi \qquad (30\text{-a})$$

$$\lambda_M = \frac{2(1-\nu^2)}{BE} \left(\frac{6}{w}\right)^2 \int_0^{\xi} \xi \, Y_M^2(\xi) \, d\xi \qquad (30\text{-b})$$

where $\xi = \frac{a_{eff}}{W}$ and $Y_F(\xi)$, $Y_M(\xi)$ are given as:

$$Y_F(\xi) = 1.99 - 0.41(\xi) + 18.70(\xi)^2 - 38.48(\xi)^3 + 53.85(\xi)^4 \quad (30\text{-c})$$

$$Y_M(\xi) = 1.99 - 2.47(\xi) + 12.97(\xi)^2 - 23.17(\xi)^3 + 24.80(\xi)^4 \quad (30\text{-d})$$

Note that Eqs. 29 and 30 are applicable only for $\xi \leq 0.6$.

For the case of non-uniformly distributed fiber bridging stress, the total F can be determined from:

$$F = B \int_0^{\ell_f} \sigma(y)\, dy \quad (31)$$

substitute $\sigma(y)$ from Eq. 28

$$F = B\,\sigma_{max} \int_0^{\ell_f} \left[1 - A_k y\right]^2 dy \quad (32)$$

$$F = B\,\sigma_{max} \cdot \ell_f \left[1 - A_k\,\ell_f + A_k^2\,\frac{\ell_f^2}{3}\right] \quad (33)$$

Note that the size of fiber bridging zone was again controlled by half the fiber length; however, in the case of notched beam specimen the value of COD was always smaller than half the fiber length. As a result, the size of ℓ_f was equal to:

for COD $\leq$ L/2 :

$$\ell_f = a - a_o \quad (34)$$

The resisting moment due to force F depends on the distance between the neutral axis and the crack tip. The problem then depends on where the

location of the neutral axis is. According to Hannant [15], the neutral axis of an unnotched fiber reinforced concrete beam is approximately one-quarter of the beam depth (or the unnotched distance) from the compressive surface. Therefore, the distance between the crack tip and the neutral axis was assumed to be equal to $(\frac{3}{4} W + \frac{a_o}{4} - a)$

The resisting moment can then be determined from:

$$M_r = B \int_0^{\ell_f} \sigma(y) \left[(\frac{3}{4} W + \frac{a_o}{4} - a) + y \right] dy \qquad (35)$$

Introducing $d_m = \frac{3}{4} W + \frac{a_o}{4} - a$, and substituting $\sigma(y)$ from Eq.28:

$$M_r = B \int_0^{\ell_f} \sigma_{max} (1 - A_k y)^2 (d_m + y) \, dy \qquad (36)$$

$$M_r = B \cdot \sigma_{max} \cdot \ell_f \left[d_m + \frac{\ell_f}{2} (1 - 2 A_k d_m) + \frac{\ell_f^2}{3} (A_k^2 d_m - 2 A_k) + \frac{A_k^2 \ell_f^3}{4} \right] \qquad (37)$$

For a given value of the applied bending moment, the dimensions of the beam and the length of the notch, a value of ℓ_p can be iterated such that the calculated value of θ from Eq. 29 is equal to η^m_{max} / ℓ_p (the value of η^m_{max} was considered from the matrix and was found to be 0.08×10^{-2} in. according to [19, 20, 21]).

Once the initiation condition is satisfied, the crack mouth displacement is calculated from:

$$CMD = \theta (a + \ell_p) \qquad (38)$$

the calculated value of CMD is then checked with the experimentally observed data. If this condition is satisfied, the assumed crack profile and the iterated ℓ_p are correct, otherwise a new crack profile is assumed and the above procedure is repeated until such displacement condition is satisfied.

Details of the test setup and the specimen dimensions for the notched beam specimen are given in Fig. 12.

CALCULATION OF FRACTURE ENERGY

The resistance to crack extension can be expressed in terms of the strain energy release rate. This term should include, in addition to the elastic energy, the energy absorbed in the fiber bridging zone (as well as in the matrix process zone, which was ignored here). In terms of the global compliance concept, the terms for strain energy release rate should include both the unloading compliance (C_R in Fig. 13) and the permanent deformation (δ_p).

To determine the actual amount of energy required for crack propagation, it has been shown that the classical concept of strain energy release rate must be modified to include the effect of nonlinear zone (in this case, the fiber bridging zone) [7, 9, 19]. It was also shown that the energy required for incremental crack growth should be the area under the load deformation curve between two unloading lines at those corresponding crack growths (shaded area in Fig. 13), i.e.,

$$G_m = \frac{P_1 P_2}{2t_n} \left[\frac{dC_R}{da_{eff}} + \left\{ \frac{P_1 + P_2}{P_1 P_2} \right\} \frac{d\,\delta_p}{da_{eff}} \right] \tag{39}$$

where P_1 and P_2 are two consecutive neighboring loads, t_n is the critical thickness in the crack plane, C_R and δ_p are the unloading (elastic) compliance and the permanent deformation, respectively. To calculate G_m from Eq. 39, it is clearly indicated that the change of unloading compliance and permanent deformation with crack growth must be determined.

During the unloading process, the fiber slipping distance or pulled-out displacement was assumed to remain constant. This behavior was experimentally observed by Hawkins, Lin and Jeang [29]. They reported that the slip in reinforced concrete during unloading remains constant (Fig. 14). It implies that the same fiber bridging pressure which resists the crack from opening during the loading process also acts as frictional force and resists the crack from closing during the unloading process. As a result, we can conclude that the existing permanent deformation at the end of the unloading period (P = 0) is equal to the load-line deformation due to fiber bridging stress which prevents the crack from opening. If the fiber bridging stress was assumed to remain constant throughout the unloading, the deformation 2 (due to fiber bridging during loading) must equal the deformation 3 (due to fiber preventing crack from closing during unloading) (Fig. 15).

To determine R-curve (fracture energy vs. crack extension) from a given set of load P and crack a, the procedure mentioned earlier for DCB and NB was used to iterate for the size of the matrix process zone and calculate the total load-line deformation (η_p) total. From the same crack closing pressure, the permanent deformation (η_p) perm can also be calculated from the elastic beam bending theory. Knowing both the permanent deformation and the total load-line displacement, the elastic deformation can be determined from Fig. 15:

$$(\eta_p)\ \text{total} = (\eta_p)\ \text{perm.} + (\eta_p)\ \text{elastic} \tag{40}$$

The unloading compliance (C_R) can then be calculated from:

$$C_R = \frac{(\eta_p)\text{elastic}}{P} \tag{41}$$

By plotting C and (η_p) perm. with crack length, the change of unloading compliance and permanent deformation with respect to crack growth can be determined. Consequently, G_m can be calculated from Eq. 39, and eventually R-curve can be obtained by plotting the obtained G_R with the actual crack growth, Δ_a.

EXPERIMENTAL INVESTIGATION

SPECIMEN CONFIGURATION

The double cantilever beam specimens (Fig. 10) used in this study were 24 in. long tapered beams developed by Visalvanich and Naaman [11]. The specimens were 2 in. thick with double grooves along the center line of the specimen which provided a 0.5 in. critical thickness. Details of the specimen setup were given in [11].

The notched beam specimens were tested by Velazco et al (30). The specimens were 1.5 in. thick with 3 in. width and a span length of 15 in. Details of the specimen and test setup are shown in Fig. 12.

MATERIAL PROPERTIES AND MIX PROPORTION

The matrix mix-proportion used in this study was (1:2:0.5) (Cement : Sand : Water). The cement used was high early strength ASTM Type III cement; the sand was a siliceous sand with a maximum particle size passing sieve No. 8 (0.0937 in. opening).

The fibers used were straight cut, brass coated steel fibers with the specific gravity of 490 lb/ft^3. Three different volume fraction of fibers, 0.5, 1 and 2 percent were selected to study the effect of fiber content. Two different sizes of fiber: 0.25 in. long with 0.006 in. diameter, and 0.75 in. long with 0.016 in. diameter, were used. In this report, four series of fiber volume fraction and aspect ratio (as listed in Table 1), with two specimens each, were theoretically studied. Only the series of V_f = 1 % with ℓ = 0.25", and d = 0.006" which were tested by the authors with the loading-unloading technique [7, 19]; all other series of DCB specimens were tested by Visalvanich [11] without the unloading process and therefore could not be used to obtain the experimental R-curves.

The notched beam tests were conducted by Velazco [30]. The data used in this study have a constant fiber volume fraction of 1 percent with the initial cast notch varied from 3/8 in. to 1.5 in. The steel fibers used were brass-coated, 1 in. long, and 0.01 in. in diameter ($\ell/_d$ = 100). The fibers specific gravity was 490 lb/ft^3, and the matrix mix-proportion was 1:2:0.5 (Cement : Sand : Water). The experimental data provided by Velazco [30] were the applied load, crack growth and the crack mouth displacement; no unloading was reported in the testing procedure.

COMPARISON WITH EXPERIMENTAL DCB DATA

Since only the series of V_f = 1 %, ℓ = 0.25", and d = 0.006" for the double cantilever beam specimens were tested with the loading-unloading technique, only the experimental R-curves of these series were then calculated and compared with the theoretical values in this section, while the results of all other series will be reported later.

With the assumed crack profile, the iterated ℓ_p was calculated by satisfying the initiation criterion (i.e., crack displacement at the end of the matrix process zone equals η^m_{max} of the matrix, Figs. 5 and 6). To ensure that the obtained ℓ_p and the assumed crack profile were correct, the predicted total load-line deformation must be in good agreement with the observed values.

Fig. 16 shows the plot of total load-line deformation $(\eta_p)_{total}$ with crack growth while Fig. 17 reports the load-deformation curves. It can be seen that the predicted values are in good agreement with the experimentally observed values. (Note that the solid points refer to the experimental data while the blank point represents the predicted values; the same notation will be used throughout this study.)

Since the fiber bridging pressure primarily resulted from the frictional bond strength and the slipping distance was assumed to remain constant during unloading [29], the permanent deformations can easily be determined from the obtained fiber bridging pressure, using the elastic beam bending concept. Fig. 18 shows a plot of permanent deformation versus crack growth and it can be seen that the predicted results are in good correlation with the experimental data.

In Fig. 19, a good correlation is also observed for the predicted and measured unloading compliances at small crack growth. The correlation is poorer at the larger crack growth. This may be because of the so-called end-effect. The end-effect in the double cantilever beam specimen is related to the size of the uncracked portion of the specimen since the DCB analyses assume the beam to be fixed at the crack tip. As a result, the smaller the uncracked ligament, the more inaccurate the fixed-end concept. For the double cantilever beam used in this study, the valid region without the end-effect is for crack growth of less than 16 in.

Knowing the change of permanent deformation and unloading compliance with crack growth (Figs. 18 and 19), R-curves can be determined from Eq. (39). The predicted R-curve was compared with the experimentally observed R-curve in Fig. 20 where good agreement was observed in general.

COMPARISON WITH OTHER DCB DATA

Other DCB experimental data which will be used for comparison with the predicted results are the series of V_f = 0.5 %, ℓ = 0.25", d = 0.006"; V_f = 2 %, ℓ = 0.25", d = 0.006"; and V_f = 1 %, ℓ = 0.75", d = 0.016".

The comparisons of the theoretically predicted load-line deformation with the experimental results reported in [11] are presented in Figs. (21a - 21c) which are the plot of load-line deformation with crack growth. It can be seen that all predicted results were in good correlation with the experimental data. This implies that the assumptions of linear crack profile and the negligibility of crack closing pressure within the matrix process zone are satisfactory. It was also found that the higher the fiber volume fraction (V_f), the larger the total load-line deformation.

The load-deformation curves predicted, using the proposed model, were found to be in good agreement with the experimentally observed values reported in [11], as can be seen in Figs. 22a - 22c.

Fig. 23 shows a plot of predicted permanent deformation for all four sets of fiber reinforced concrete. It was observed that the higher the volume fraction, the longer the predicted permanent deformation. It can also be seen that the larger the value of fiber aspect ratio, the larger the permanent deformation. The rate of change in permanent deformation (with respect to crack growth also increased with fiber volume fraction and aspect ratio.

A plot of unloading compliance with crack growth for all four sets of fiber reinforced concrete was shown in Fig. 24. For V_f = 0.5 %, the predicted C_R-a relationship was close to linear. It was also observed that the larger the amount of fibers (higher volume fraction), the more nonlinear behavior exists for the unloading compliance and crack growth relationship.

Fig. 25 shows the comparison of the predicted R-curves for all four series of fiber reinforced concrete. It can be seen that increasing the amount of fibers (volume fraction) resulted in an increase in the fracture resistance. For the same volume fraction, increasing the fiber aspect ratio (length) also increased the fracture toughness of the composites.

Note that if the asymptotic value of the R-curve is considered as a material parameter, then that value can be a useful quantity in identifying the benefit of fiber addition. For example, by comparing the R-curves of specimens reinforced with 0.75 in. long fibers and plain mortar, it can be observed that the asymptotic steady-state value of fracture energy is

increased more than 40 times due to fiber addition. This relative value is somewhat comparable with the reported value of "toughness index" (relative values of areas under the load-deflection curve in flexure) by other investigators [33, 34, 35]. Thus, the model proposed here seems to provide a tool for predicting the effectiveness of fibers in improving the fracture resistance of concrete.

COMPARISON WITH EXPERIMENTAL NOTCHED BEAM DATA

Using the theoretical model proposed for the notched beam specimens, the theoretical load-crack mouth displacement relationships were predicted for plain mortar and fiber reinforced concrete (Fig. 26). The mix-proportion for plain mortar was 1:2:0.5 (Cement : Sand : Water). Three different sets of initial notch a_o with V_f equalled to 1 percent and "σ_{max} = 300 psi" were studied.

A good correlation is observed for the predicted and the measured crack mouth displacement for plain mortar (Fig. 26). These results were calculated using the observed peak loads and the initial crack length from [30].

For fiber reinforced concrete, the comparisons in Fig. 26 show that the analysis does not correlate exactly with the experimental results. However, the predicted values were still in good agreement with the observed data. These variations may be attributed to the fact that: 1) the actual neutral axis for the notched-fiber reinforced beam is not known, the neutral axis used in this analysis was based on what has been proposed by Hannant [15]-- ($d/_4$ from the compression face where d is the depth of the unnotched beam); 2) the theoretical concept proposed by Okamura et al

[27, 28] is valid only when the $a/_w$ ratio is less than 0.6, with fiber reinforced concrete, most observed crack growths reported in Ref. [30] had $a/_w$ much larger than 0.6. The assumed linear crack profile might not be accurate enough for the case of notched beam specimens which leads to a wrong estimation of the fiber bridging pressure.

Additional theoretical analysis for predicting crack mouth displacement more accurately for notched beam specimens is currently under way.

MATRIX PROCESS ZONE, FIBER BRIDGING ZONE AND CRITICAL COD

The value of the matrix process zone ℓ_p can only be obtained through the iteration procedure which must satisfy the initiation criterion that the crack tip opening displacement equals η^m_{max} used here for the matrix was 0.08×10^{-2} in., as reported in References [19, 20, and 21]. The fiber bridging zone was calculated from the assumed crack profile with the condition that fibers will be completely pulled out when the crack surface displacement equals η^f_{max} (half the fiber length, Fig. 6). In this study, since the value of crack opening displacement was always less than η^f_{max} (half the fiber length), the size of the fiber bridging zone was then equal to the crack length subtracted by the length of the initial cast notch.

Fig. 27 shows the plot of both the calculated matrix process zone and the fiber bridging zone (ℓ_p and ℓ_f, respectively) for the DCB specimens. It can be observed that the matrix process zone is essentially constant with respect to crack growth. The value of ℓ_p calculated from fiber reinforced mortar specimen was almost identical to those obtained from mortar specimens [19, 20, 21]. The conclusion of constant process zone was also confirmed in other materials like DMMA [31, 32]. The obtained value of ℓ_p was found to

be approximately about 3 in. and seemed to be independent of different fiber volume fraction and aspect ratio (Fig. 27).

A plot of the matrix process zone and the fiber bridging zone with the uncracked ligament in the notched beam specimens is shown in Fig. 28. The predicted matrix process zones, using the proposed model, were found close to what has been reported for the unreinforced mortar [19, 20]. Fig. 18 also shows that the fiber bridging zone increases with crack growth, or as the uncracked ligament decreases.

Table 1. PREDICTED STRESS-DISPLACEMENT RELATIONSHIPS FOR DIFFERENT V_f AND ℓ/d FOR DCB SPECIMENS

V_f %	ℓ/d	ℓ (in.)	d (in.)	$\sigma - \eta$ relationship ** (psi)
0.5	41.67	0.25	0.006	$\sigma = 125\ (1 - 8\eta\ )^2$
1.0	41.67	0.25	0.006	$\sigma = 250\ (1 - 8\eta\ )^2$
1.0	46.88	0.75	0.016	$\sigma = 281.28\ (1 - 2.67\eta\ )^2$
2.0	41.67	0.25	0.006	$\sigma = 500\ (1 - 8\eta\ )^2$

** These stress-displacement relationships were predicted, using βr = 600 psi, and the proposed normalized relationship (Eq. 15)

REFERENCES

1 Mai, Y. W., "Strength and Fracture Properties of Asbestos-Cement Mortar Composites," Journal of Materials Science, Vol. 14, No. 9, September 1979, pp. 2091-2102.

2 Lenian, J. C., and Bunsell, A. R., "The Resistance to Crack Growth of Asbestos Cement," Journal of Materials Science, Vol. 14, 1979, pp. 321-332.

3 Foote, R. M. L., Cotterell, B., and Mai, Y. W., "Crack Growth Resistance Curve for a Cement Composite," in Advances in Cement Matrix Composites, Proceedings, Symposium L, Materials Research Society, Annual Meeting, Boston, Massachusetts, Nov. 17-18, 1980, pp. 135-144.

4 Bowling, J., and Groves, G. W., "The Propagation of Cracks in Composites Consisting of Ductile Wires in a Brittle Matrix," Journal of Materials Science, Vol. 14, 1979, pp. 443-449.

5 Mindess, S., Lawrence, F. V., and Kesler, C. E., "The J-Integral as a Fracture Criterion for Fiber Reinforced Concrete," Cement and Concrete Research, Vol. 7, 1977, pp. 731-742.

6 Velazco, G., Visalvanich, K., and Shah, S. P., "Fracture Behavior and Analysis of Fiber Reinforced Concrete Beams," Cement and Concrete Research, Vol. 10, Jan. 1980, pp. 41-51.

7 Wecharatana, M., and Shah, S. P., "Slow Crack Growth in Cement Composites," Proceedings of ASCE, Journal of Structural Division, Vol. 108, No. ST6, June 1982, pp. 1400-1413.

8 Mai, Y. W., and Cotterell, B., "Slow Crack Growth and Fracture Instability of Cement Composites," International Journal of Cement Composites and Lightweight Concrete, Vol. 4, No. 1, Feb. 1982.

9 Wecharatana, M. and Shah, S. P., "Double Torsion Tests for Studying Slow Crack Growth of Portland Cement Mortar," Cement and Concrete Research, Vol. 10, No. 6, Nov. 1980, pp. 833-844.

10 Dugdale, D. S., "Yielding of Steel Sheets Containing Slits," Journal of Mechanics, Physics and Solids, Vol. 8, 1960, pp. 100-104.

11 Visalvanich, K., "Fracture Modelling for Fiber Reinforced Concrete," Ph.D. Dissertation, Department of Materials Engineering, University of Illinois at Chicago Circle, Chicago, Illinois, February 1982.

12 Petersson, P. E., "Fracture Mechanical Calculations and Tests for Fiber-Reinforced Cementitious Materials," in Advances in Cement-Matrix Composites, Proceedings, Symposium L, Materials Research Society, Annual Meeting, Boston, Massachusetts, Nov. 17-18, 1980, pp. 95-106.

13 Hillerborg, A., "Analysis of Fracture by Means of the Fictitious Crack Model, Particularly for Fiber Reinforced Concrete," International Journal of Cement Composites, Vol. 2, No. 4, Nov. 1980, pp. 177-184.

14 Paris, P. C., and Sih, G. C. M., "Stress Analysis of Cracks," in Fracture Toughness Testing and its Application, ASTM-STP 381, ASTM, Philadelphia, 1964, pp. 30-83.

15 Hannant, D. J., "Fiber Cements and Fiber Concretes," John Wiley & Sons, New York, 1978.

16 Muskelishvili, N. I., "Some Basic Problems of the Mathematical Theory of Elasticity," Noordhoff International, Leyden, 1976.

17 Wiederhorn, S. M., Short, A. M., and Moses, R. L., Journal of Applied Physics, Vol. 39, 1968, pp. 1569.

18 Barenblatt, G. J., "The Mathematical Theory of Equilibrium Crack in the Brittle Fracture," Advances in Applied Mechanics, Vol. 7, 1962, pp. 55-125.

19 Wecharatana, M., "Fracture Resistance in Cementitious Composites," Ph.D. Dissertation, Department of Materials Engineering, University of Illinois at Chicago Circle, Chicago, Illinois, March 1982.

20 Wecharatana, M., and Shah, S. P., "Predictions of Nonlinear Fracture Process Zone in Concrete," Submitted for possible publication in ASCE, Engineering Mechanics Division, 1982.

21 Wecharatana, M., and Shah, S. P., "Experimental Methods to Determine Fracture Parameters for Concrete," Presented at the Seminar of Fracture Mechanics, Domaine de Saint-Paul, B. P. 1, 78470, Saint-Remy-les-Chevreuse, France, 1982, June 8-11.

22 Shah, S. P., Stroeven, P., Dalhuisen, D., and Stekelenberg, P. van, "Complete Stress-Strain Curves for Steel Fiber Reinforced Concrete in Uniaxial Tension and Compression," Proceedings, International Symposium, RILEM-ACI-ASTM, Sheffield, Sept. 1978, pp. 399-408.

23 Naaman, A. E., Moavenzadeh, F., and McGarry, F. J., "Probabilistic Analysis of Fiber Reinforced Concrete," Proceedings of ASCE, Engineering Mechanics Division, Vol. 100, No. EM2, April 1974, pp.397-413.

24 Swamy, R. N., Manget, P. S., and Rao, S. V. K., "The Mechanics of Fiber Reinforcement of Cement Matrices," Fiber Reinforced Concrete, ACI Publication SP-44, pp. 1-28.

25 Aveston, J., Mercer, R. A., and Sillwood, J. M., "Fiber Reinforced Cements - Scientific Foundations for Specifications Composites Standards Testing and Design," National Physical Laboratory Conference Proceedings, April 1974, pp. 93-103.

26 Harris, B., Varlow, J., and Ellis, C. D., "The Fracture Behavior of Fiber Reinforced Concrete," Cement and Concrete Research, Vol. 2, 1972, pp. 447-461.

27 Okamura, H., Watanabe, K., and Takano, T., "Deformation and Strength of Cracked Member Under Bending Moment and Axial Force," Engineering Fracture Mechanics, Vol. 7, 1975, pp. 531-539.

28 Okamura, H., Watanabe, K., and Takano, T., "Applications of the Compliance Concept in Fracture Mechanics," ASTM-STP 536, ASTM, Philadelphia, 1973, pp. 423-438.

29 Hawkins, N. M., Lin, I. J., and Jeang, F. L., "Load Bond Strength of Concrete for Cyclic Reversed Loadings," Proceedings of the International Conference on "Bond in Concrete," Edited by P. Bartos, Paisley College of Technology, Scotland, June 14-16, 1982.

30 Velazco, G., "Fracture Behavior and Analysis of Fiber Reinforced Concrete Beam," Master Degree Thesis, Department of Materials Engineering, University of Illinois at Chicago Circle, Chicago, Illinois, 1979.

31 Döll, W., and Weiman, G. W., "Deformationsverhalten von PMMA _ Crazes an Ribspitzen," Progress in Colloid and Polymer Science, Vol. 66, 1979, pp. 291-298.

32 Schinker, M. G., and Döll, W., "Interference Optical Measurements of Large Deformations at the Tip of a Running Crack in a Glassy Thermoplastic," in Mechanical Properties of Materials at High Rates of St Strain, Ed., J. Harding, Inst. Phys. Conf. Ser., No. 47, Chapter 2, 1979, pp. 224-232.

33 Henager, C. H., "A Toughness Index for Fiber Concrete," RILEM Symposium 1978, Sheffield, pp. 79-86.

34 Johnston, C. D., "Definition and Measurement of Toughness Parameters for Fiber Reinforced Concrete," University of Calgary, Calgary, Alberta, Canada. To be published.

35 Zollo, R. F., Fibrous Concrete Testing Technique," ACI Journal, Proceedings, Vol. 77, No. 5, Sept.-Oct. 1980, pp. 363-362.

APPENDIX I - NOTATIONS

A	cross sectional area
A_1	a factor for composite strength that related to the extent of matrix cracking
A_2	a factor for composite strength that related to fiber bridging ($= 4\ \eta_\ell\ \eta_\theta\ \tau$)
A_k	a constant obtained from the ratio of CMD/$(a - \eta^f_{max})$
a	crack length
a_o	traction-free crack length
a_{eff}	effective crack length ($= a + \ell_p$)
B	beam thickness
b, c	boundaries of the zone of uniform crack closing pressure
C	compliance ($= \delta/_p$)
C_1	*DCB - beam depth at free end*
C_2	slope of the tapered DCB specimen
C_R	unloading - reloading compliance
CMD	crack mouth displacement
COD	crack opening displacement
d	diameter of fiber
d_m	distance from crack tip to the assumed neutral axis
E	modulus of elasticity
F	total axial force in notched beam specimen
G	shear modulus of elasticity
G_c	critical strain energy release rate
G_m	modified strain energy release rate
G_R	strain energy release rate - resistance curve

$H(0)$	DCB - beam depth at crack tip
$H(x)$	DCB - beam depth at x
I	moment of inertia
k	average shear constant
K_a	stress intensity factor due to applied force P
K_c	critical stress intensity factor
K_o	stress intensity factor at crack tip calculated without considering the presence of fibers
K_R	stress intensity factor for crack porpagation in fiber reinforced matrix
K_r	stress intensity factor due to fiber bridging
K_w	stress intensity factor due to wires bridging
K_{IC}	critical stress intensity factor under mode I opening
ℓ , L	fiber length
ℓ_f	zone of fiber bridging
ℓ_p	microcracked zone or matrix process zone
$\frac{\ell}{d}$	fiber aspect ratio
M	applied moment
m, n	exponential constants for variation of fiber pulled-out behavior
P	applied load
P_1, P_2	two consecutive neighboring loads in the loading sequence
t_n	critical beam thickness in the crack plane
u_o	crack-surface displacement of a crack without fiber bridging

u_r crack-surface displacement due to fiber bridging

V shear force

V_f volume fraction of fibers

V_m percent volume of matrix

W depth of notched beam specimen

x distance from crack tip

y distance from crack tip in fiber bridging zone of notched beam specimen

$y_p(x)$ crack-surface displacement at distance x from crack tip due to applied force

$Y_F(\xi)$, $Y_M(\xi)$ polynomial functions due to force and moment in terms of ξ for notched beam specimen

α a factor (less than unity) for the effective process zone

β efficiency factor due to fiber distribution and embedment length

σ uniform crack closing pressure

σ_m tensile strength of matrix

σ_{max} maximum post-cracking strength of fiber reinforced composites

$\sigma(t)$ non-uniform crack closing pressure

$\sigma(y)$ crack closing pressure at distance y in notched beam specimen

$(\sigma_c)_{max}$ maximum strength of fiber reinforced composites

η crack-surface displacement

η_ℓ efficiency factor for the embedment length of fibers

η_θ coefficient for fiber distribution and orientation

η_p load-line deformation

$(\eta_p)_{elastic}$ elastic load-line deformation (reversible)

$(\eta_p)_{perm}$	permanent load-line deformation (irreversible)
$(\eta_p)_{total}$	total load-line deformation
η^f_{max}	maximum pulled-out displacement of fiber reinforced matrix (= half the fiber length)
η^m_{max}	maximum displacement of matrix in the descending branch of the uniaxial tensile test
τ	shear strength of matrix and fiber interface
ξ	effective crack over depth ratio in notched beam specimen (= $\frac{a_{eff}}{W}$)
δ_p	permanent deformation
θ	relative beam rotation of the crack front in notched beam specimen
λ_{FM}, λ_M	increments of the compliances caused by the pressure of force and moment, respectively
$\phi(Z)$	Muskhelishvili's pentential function
ν	Poissons' ratio

APPENDIX II - LIST OF FIGURES

Fig. 20 Experimental and Theoretical G_R - Curves - DCB :
(V_f = 1%, L = 0.25", D = 0.006")

Fig. 21 Experimental and Theoretical Load-Line Deformation and Crack Growth Relationships :
a) V_f = 0.5%, L = 0.25", d = 0.006"
b) V_f = 2% , L = 0.25", d = 0.006"
c) V_f = 1% , L = 0.75", d = 0.016"

Fig. 22 Experimental and Theoretical Load-Deformation Curves :
a) V_f = 0.5%, L = 0.25", d = 0.006"
b) V_f = 2% , L = 0.25", d = 0.006"
c) V_f = 1% , L = 0.75", d = 0.016"

Fig. 23 Comparison of Theoretical Permanent Deformation for Different Fiber Volume Fraction and Aspect Ratio.

Fig. 24 Comparison of Theoretical Unloading Compliance for Different Fiber Volume Fraction and Aspect Ratio.

Fig. 25 Comparison of Theoretical Strain Energy Release Rate for Different Fiber Volume Fraction and Aspect Ratio.

Fig. 26 Comparison of Experimental and Theoretical Load-Crack Mouth Displacement in Notched Beam Specimens.

Fig. 27 Matrix Process Zone and Fiber Bridging Zone in Fiber Reinforced Concrete - DCB Specimens.

Fig. 28 Matrix Process Zone and Fiber Bridging Zone in Fiber Reinforced Concrete - Notched Beam Specimens.

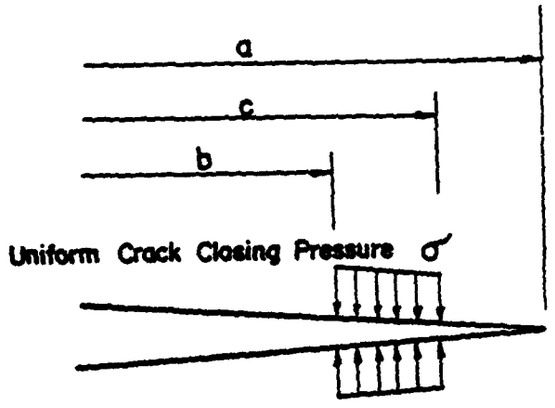

Fig. 1-a Uniform Crack Closing Pressure Applied on a Crack in an Infinite Infinite Sheet Paris and Sih

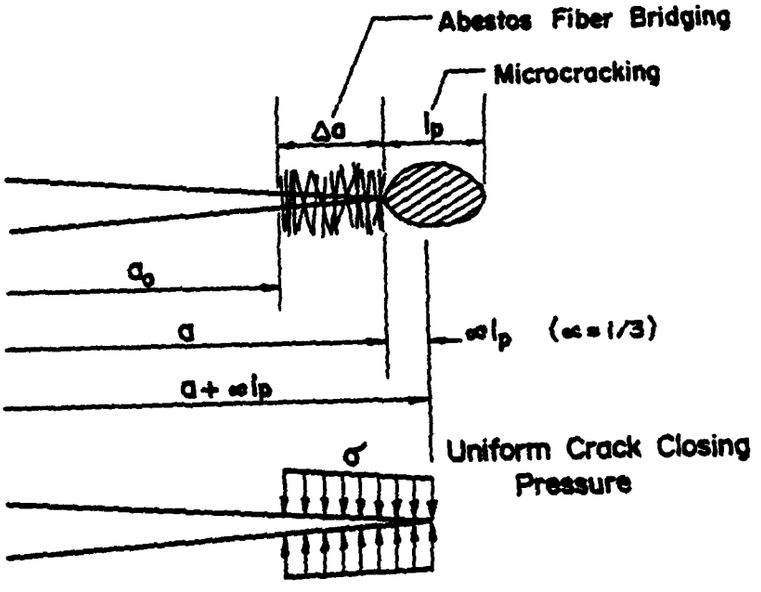

Fig. 1-b Assumed Uniform Crack Closing Pressure due to Fiber Bridging and Microcracking in a Cracked Asbestos-Cement Specimen Lenian and Bunsell

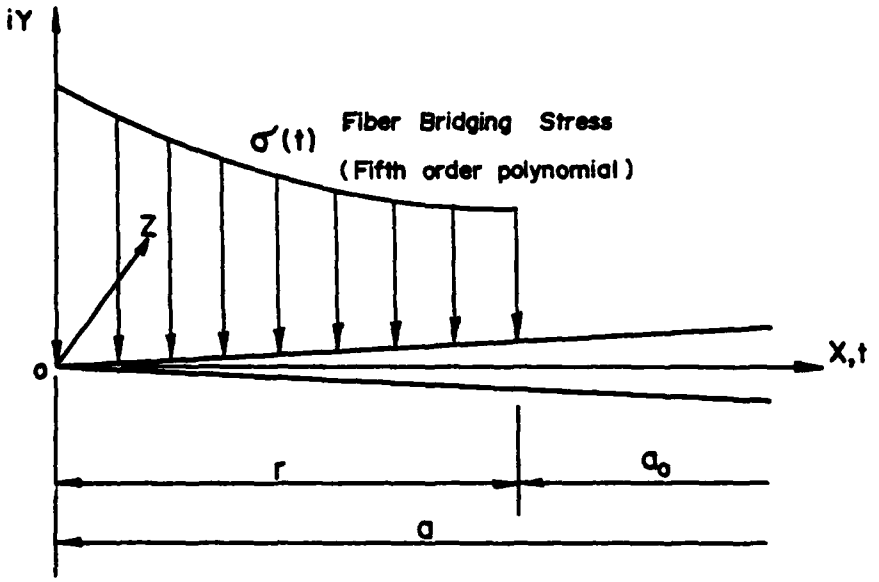

Fig. 2 Semi-Infinite Crack Model with an Assumed Fiber Bridging Stress - $\sigma(t)$ Foote, Cotterell and Mai

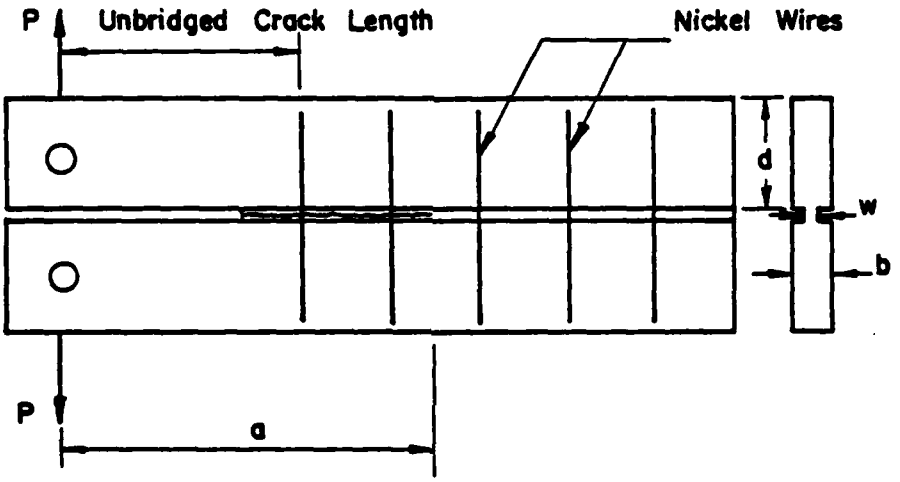

Fig. 3 Double Cantilever Epoxy Beam Reinforced with Aligned Nickel Wires Bowling and Groves

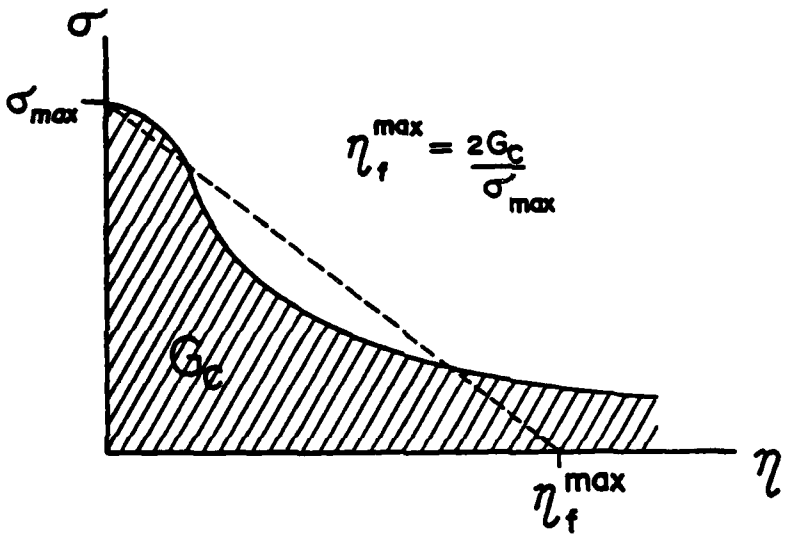

Fig. 4 Assumes Linear Stress-Displacement Relationship Compared to that Obtained from Uniaxial Tensile Test Pettersson and Hillerborg

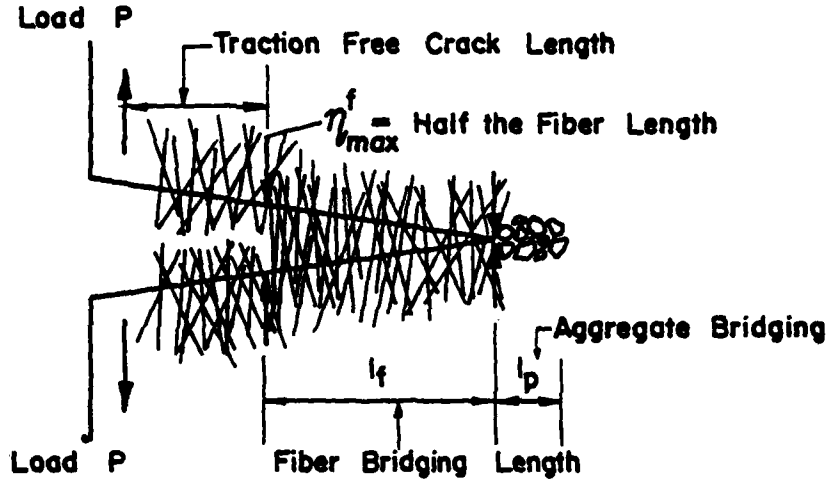

FIBER REINFORCED MATRIX

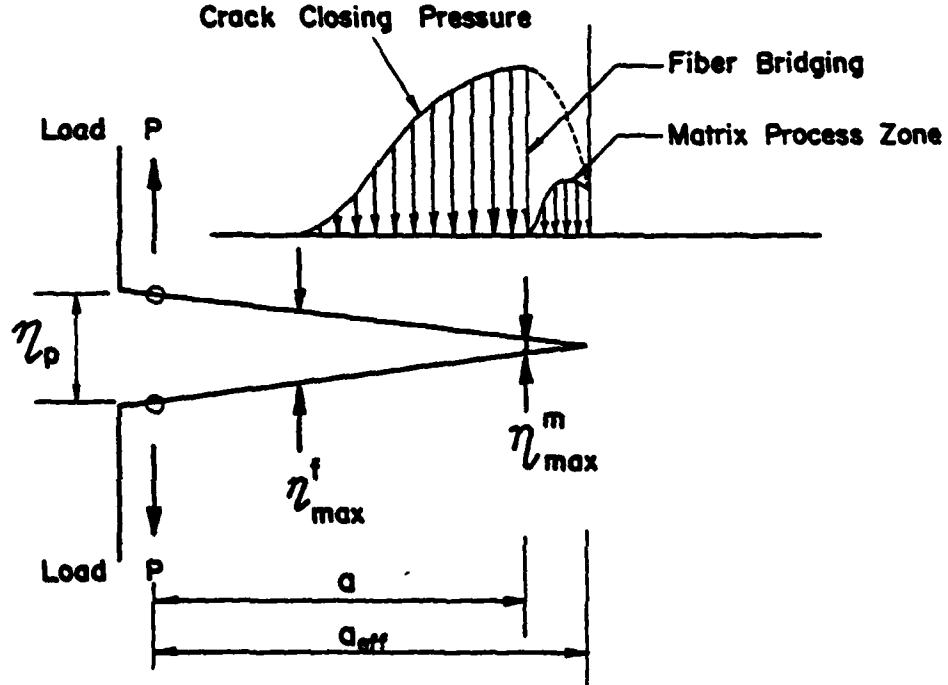

AN IDEALIZED MODEL OF PROCESS ZONE

Fig. 5 Fracture Model for Fiber Reinforced Concrete

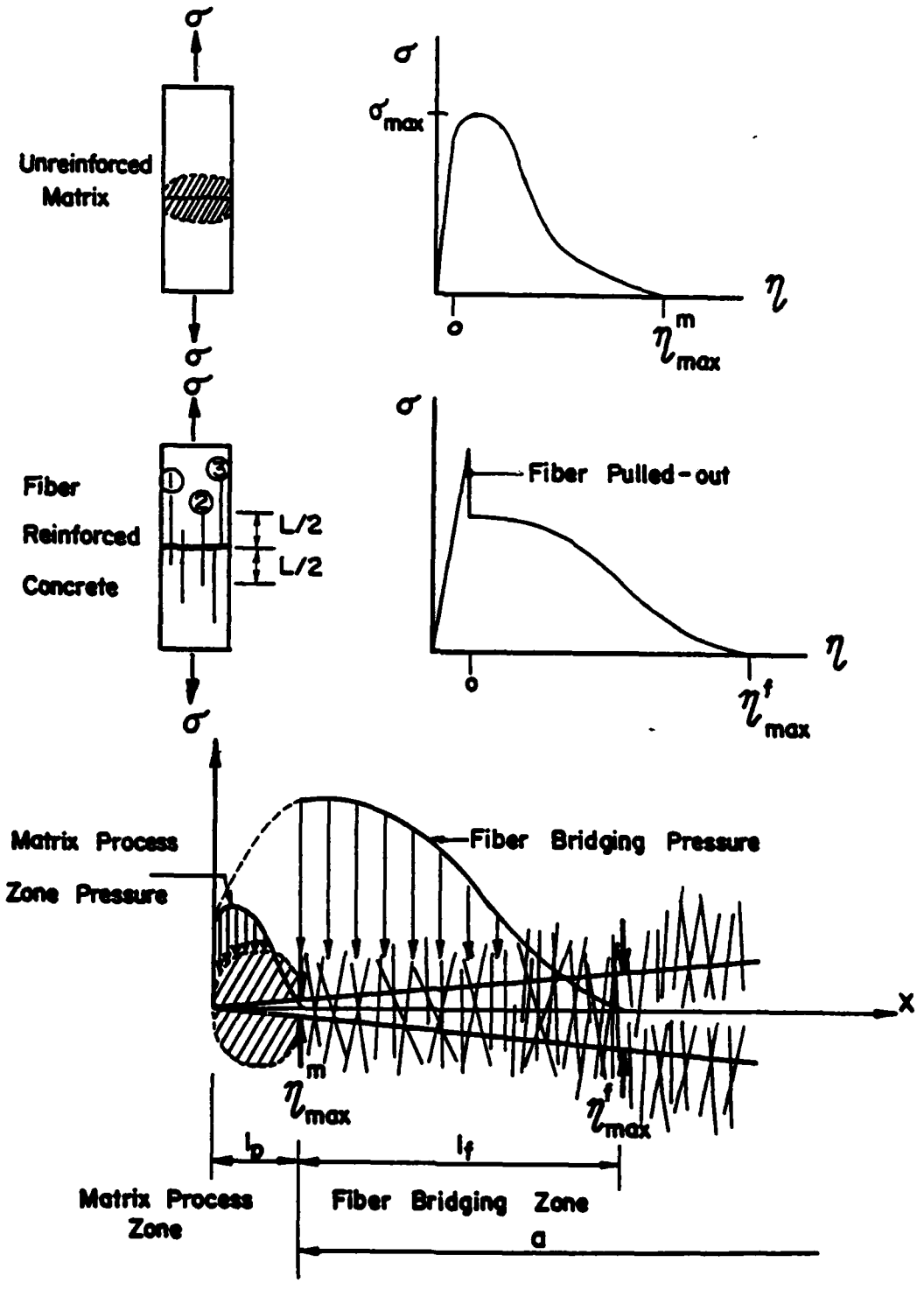

Fig. 6 Uniaxial Tensile Behaviors and Crack Closing Stress Distribution

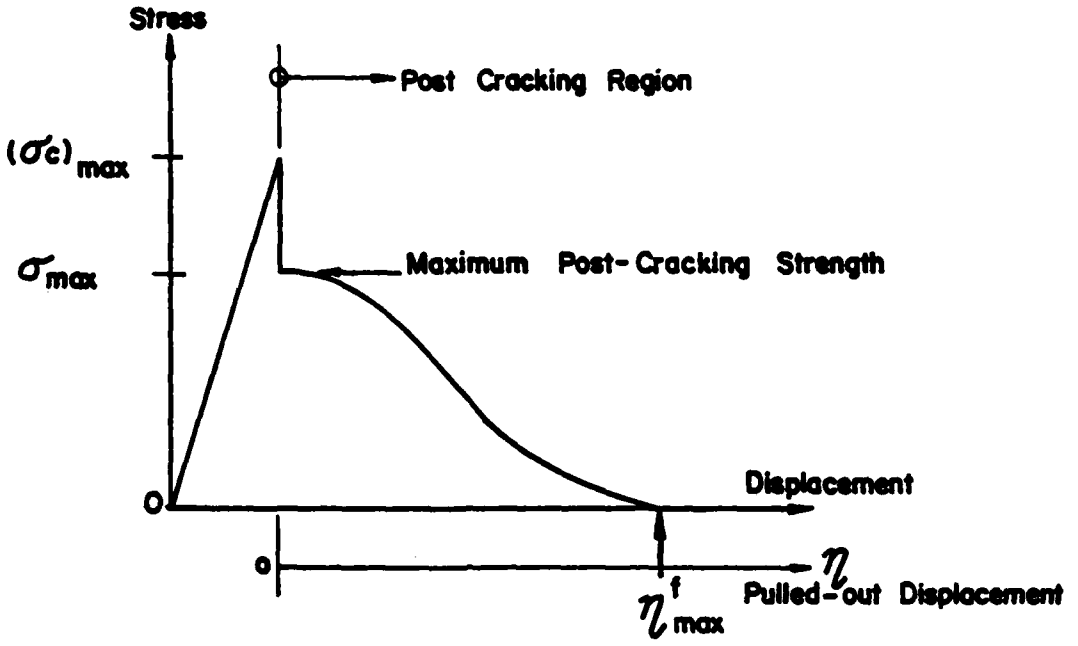

Small Fiber Volume Fraction

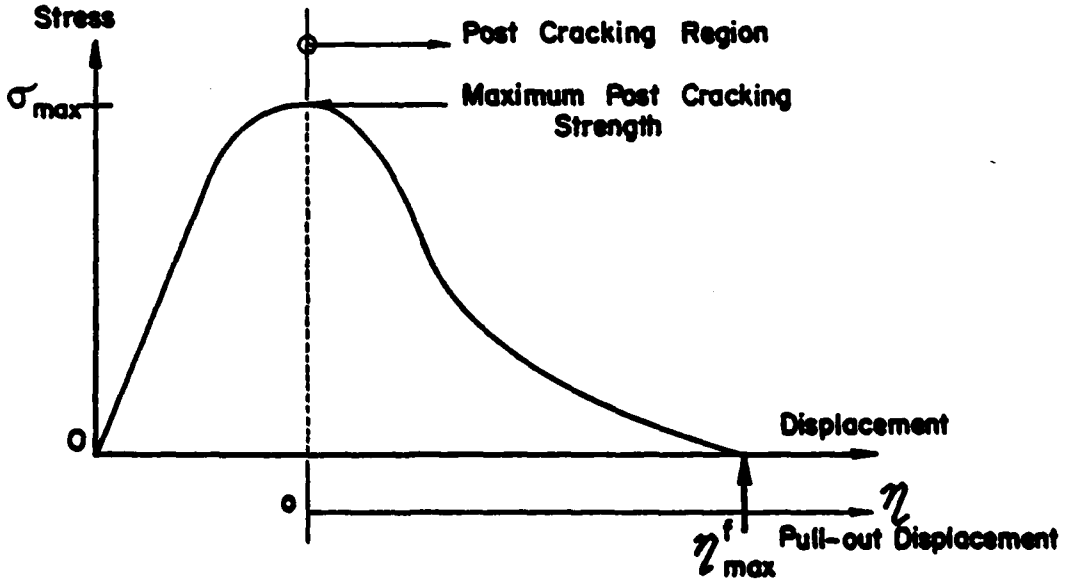

Large Fiber Volume Fraction

Fig. 7 Uniaxial Tensile Behavior of Fiber Reinforced Concrete

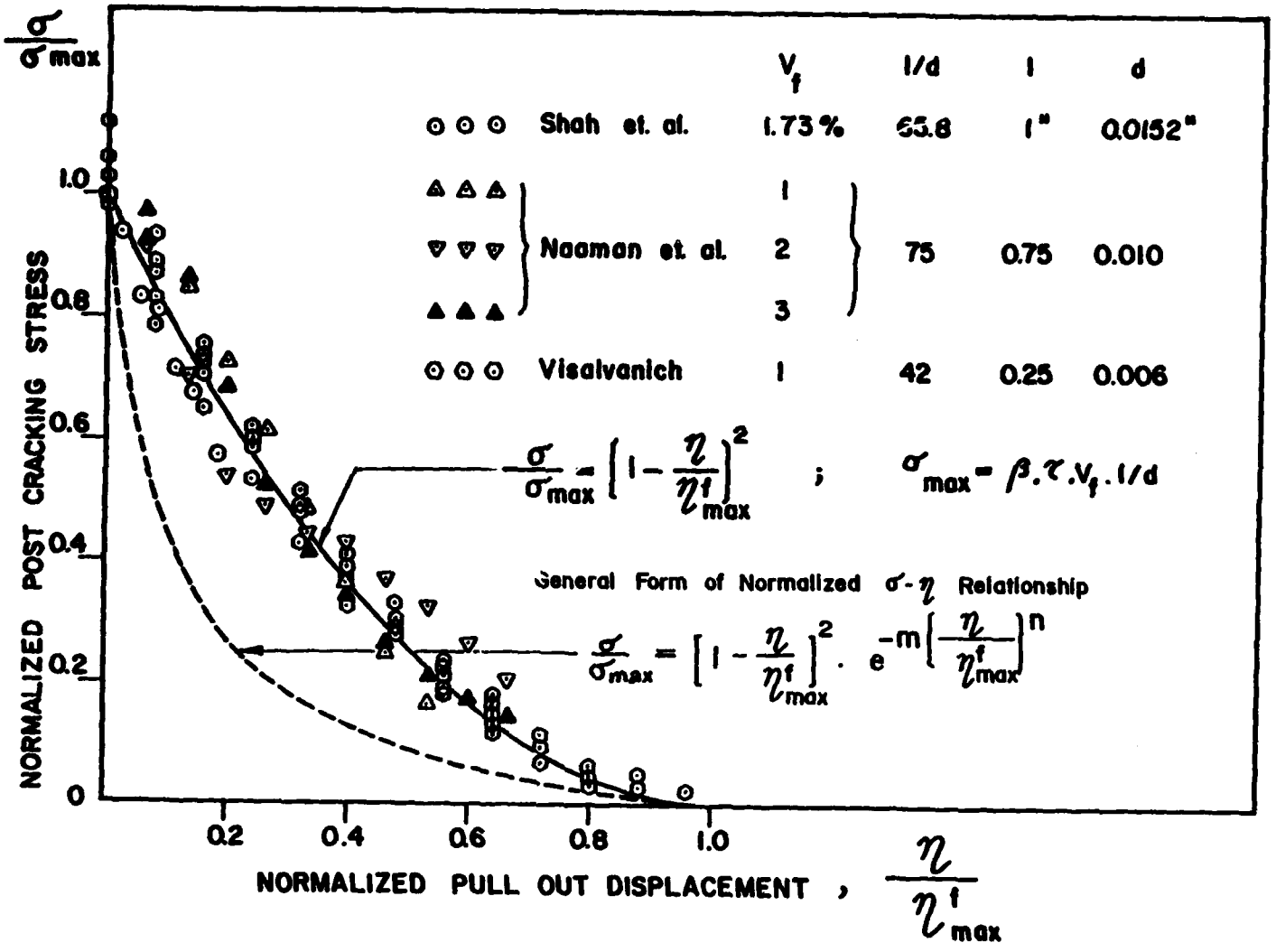

Fig. 8 Normalized Post-Cracking Tensile Stress-Displacement Relationship

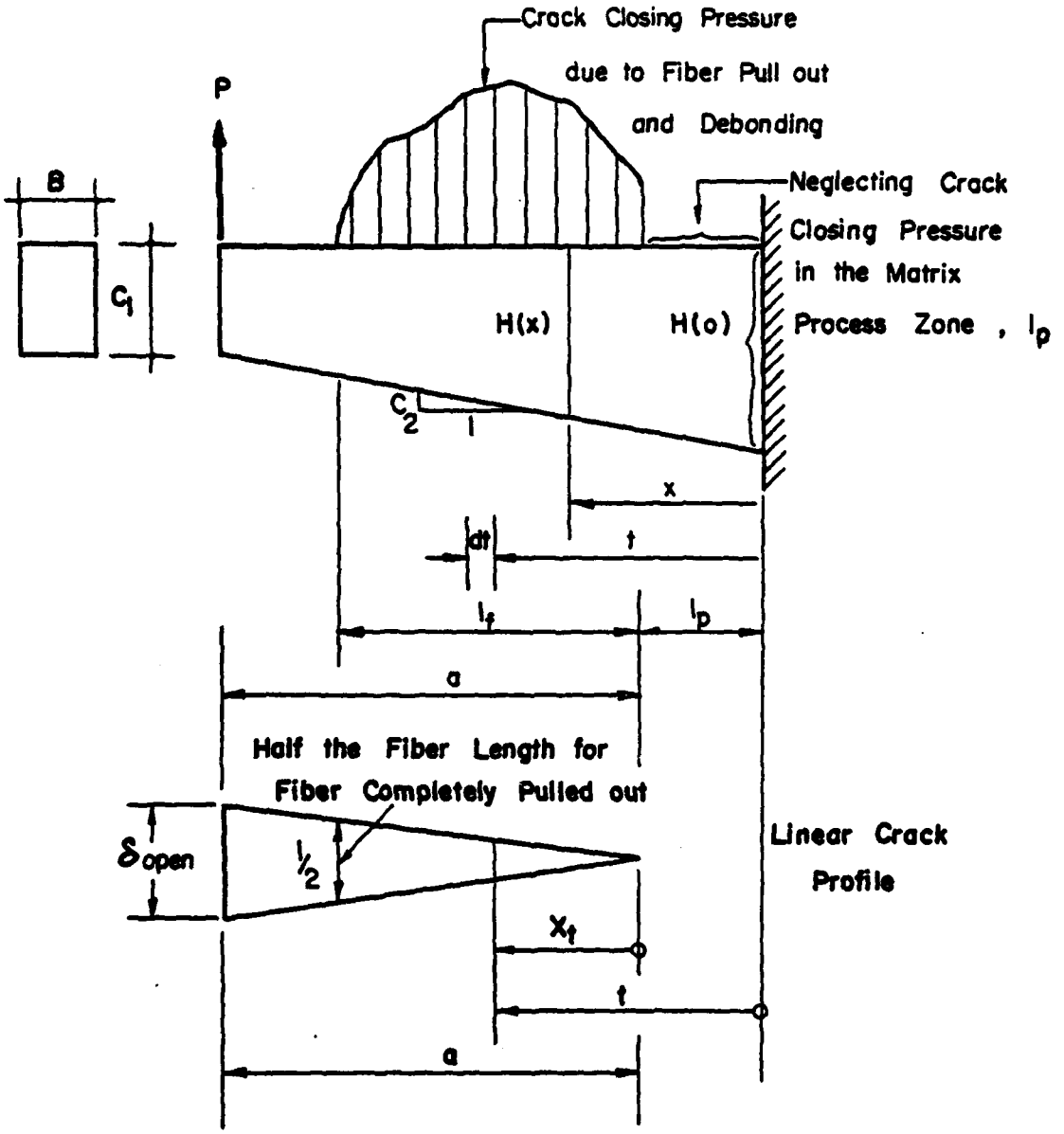

Fig.9 A Single Cantilever Beam and the Applied Loads

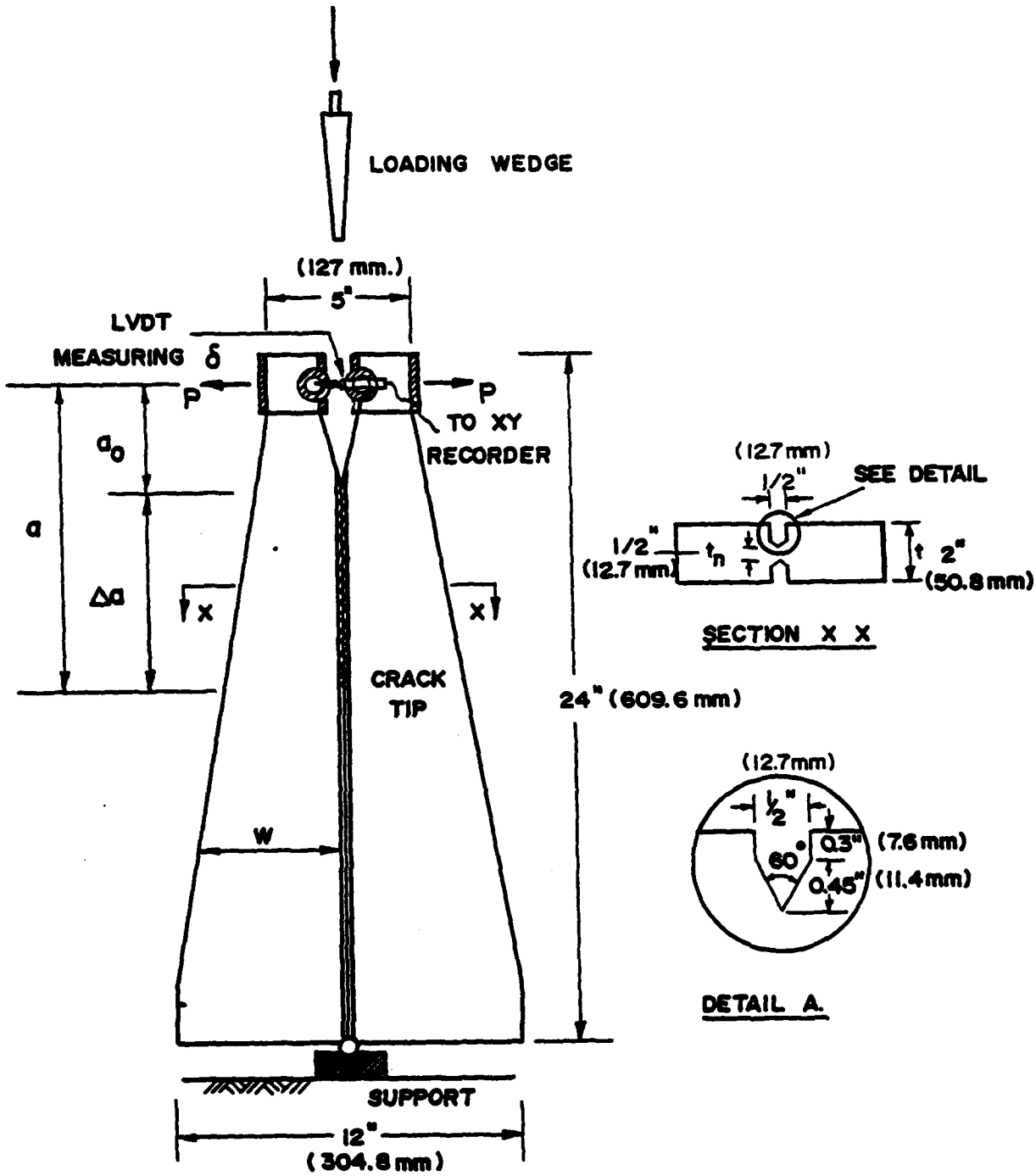

DOUBLE CANTILEVER BEAM

Fig. 10 Double Cantilever Beam; Test Setup

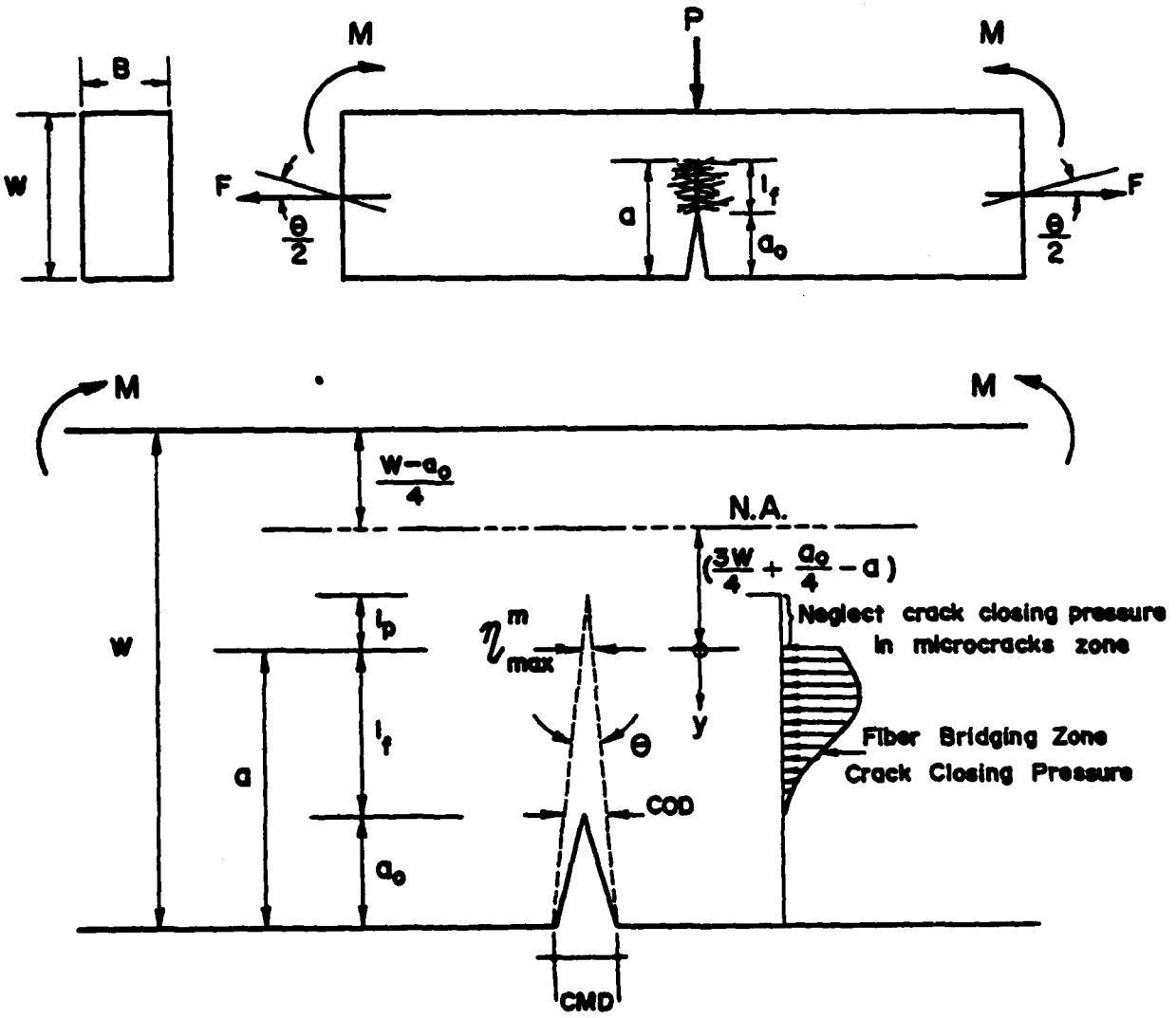

Fig. 11 A Model for Fiber Reinforced Concrete; Notched Beam Specimen

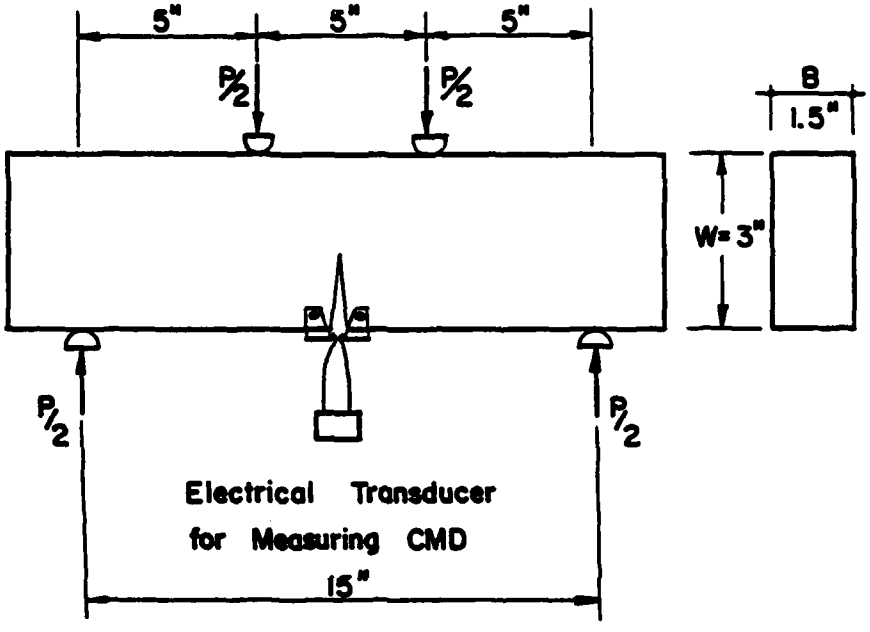

Fig. 12 Dimensions and Test Setup; Notched Beam Specimen

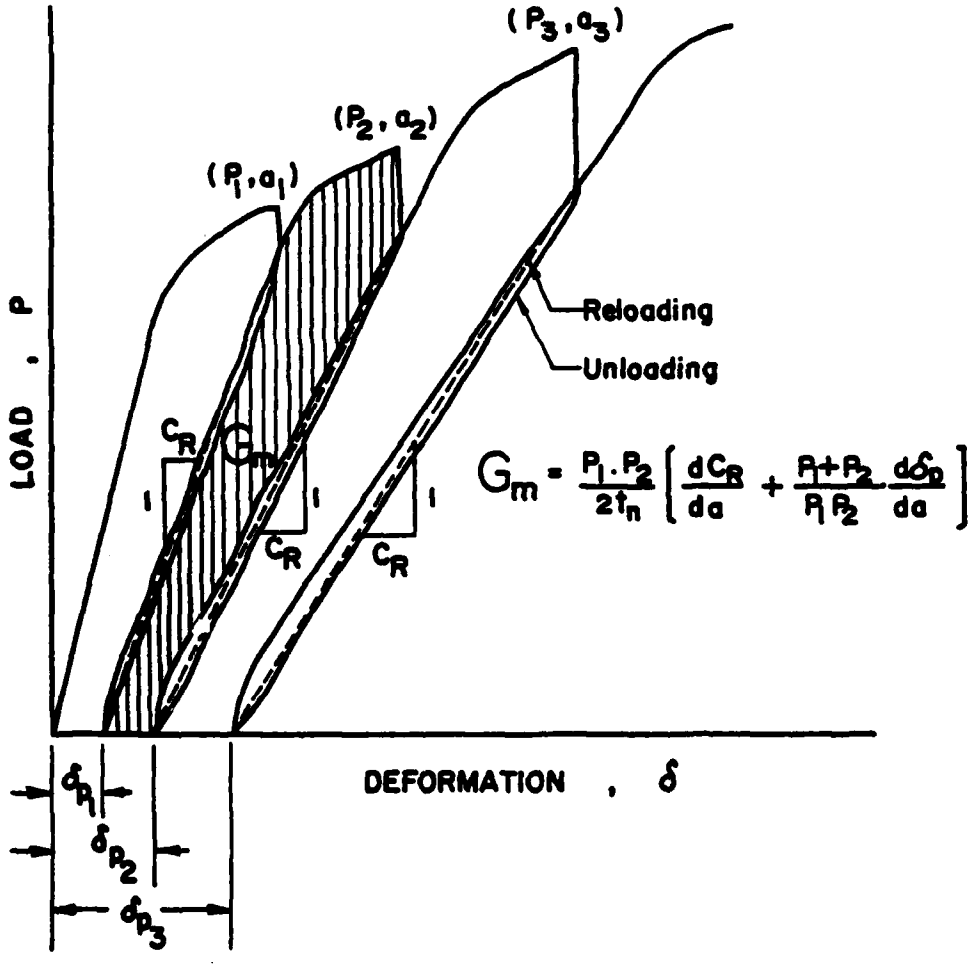

Fig. 13 Concept of Modified Strain Energy Release Rate

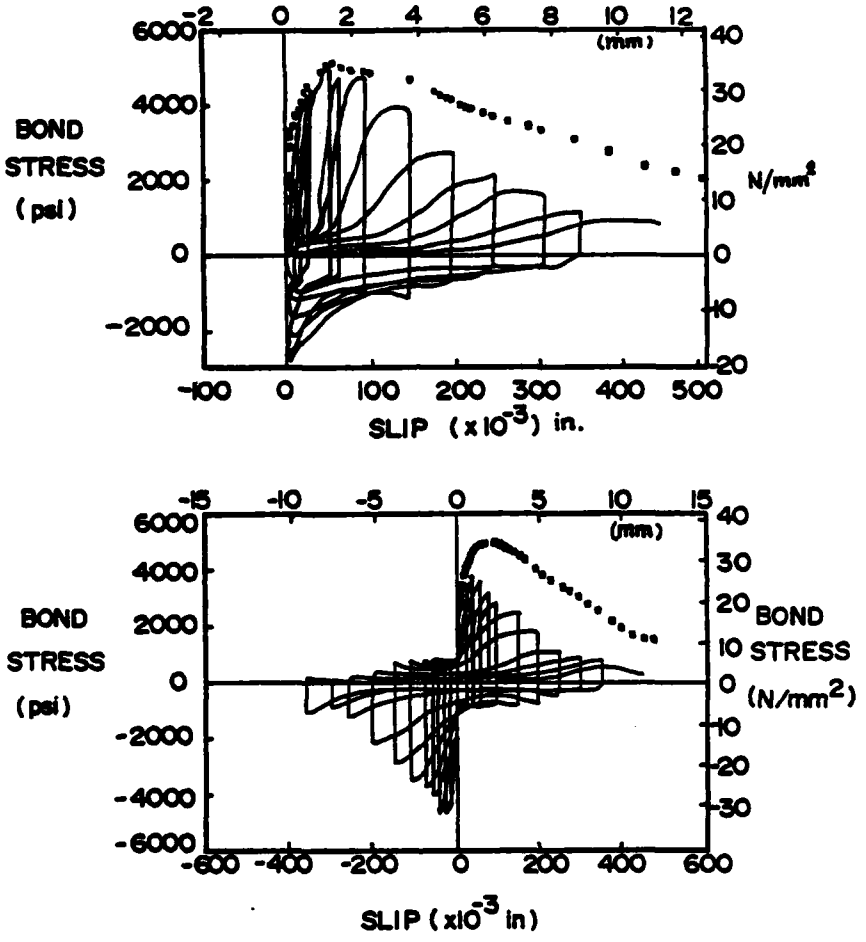

Fig. 14 Bond Stress vs. Slip Relationships in Reinforced Concrete Hawkins et al

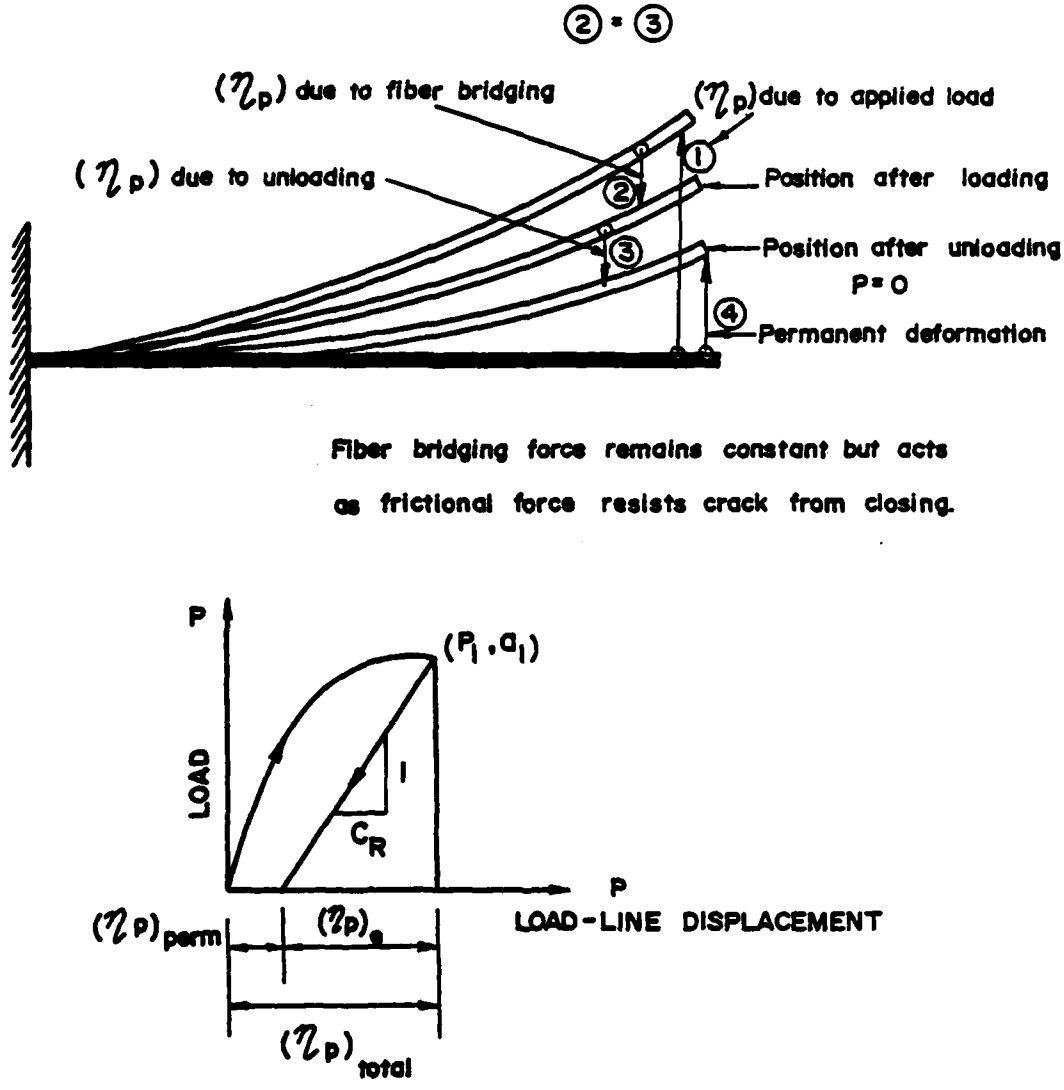

Fig. 15 Characteristic of Load-Line Deformation

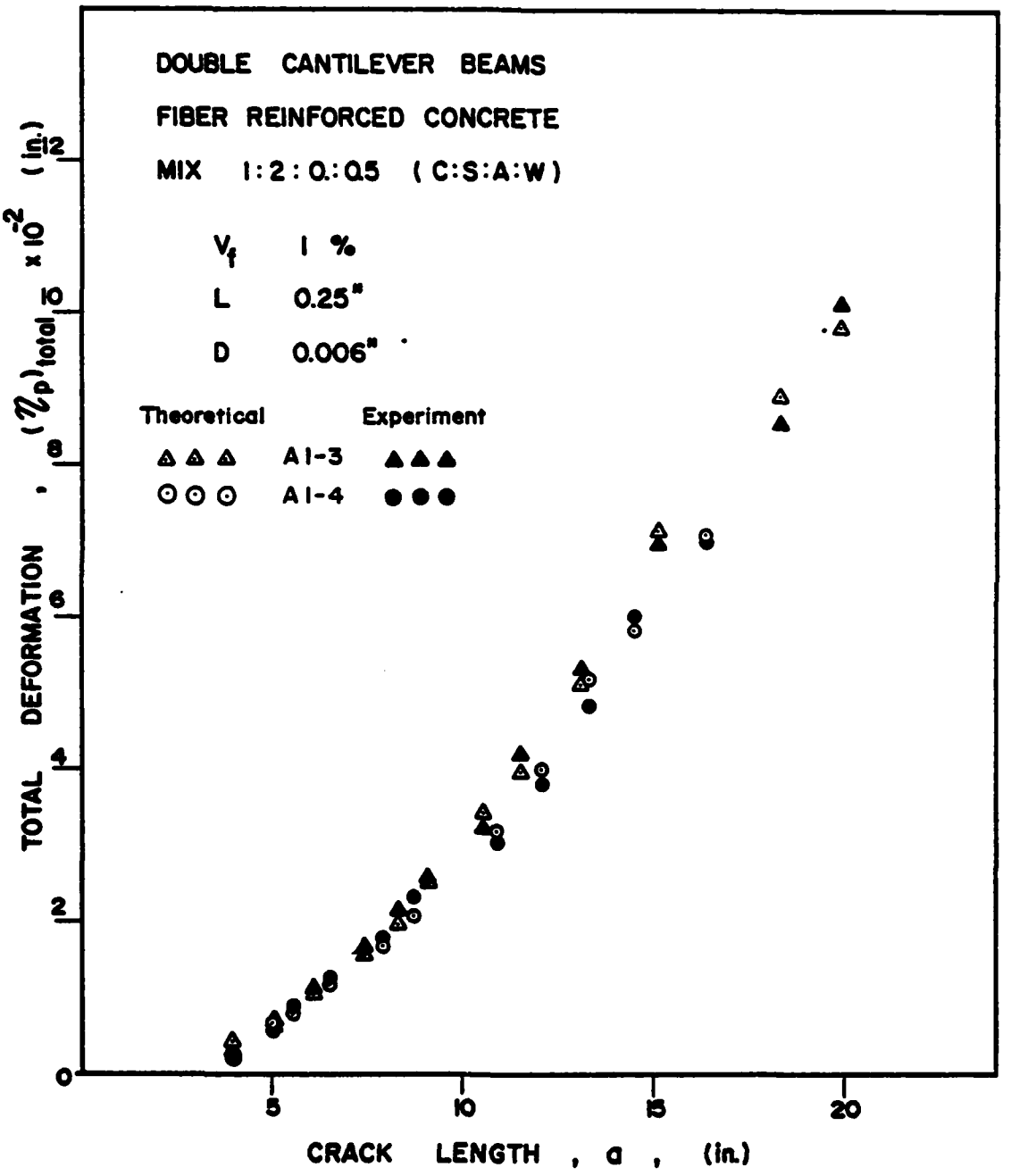

Fig. 16 Comparison of Experimental and Theoretical Load-Line Deformation vs. Crack Growth for Fiber Reinforced Concrete - DCB

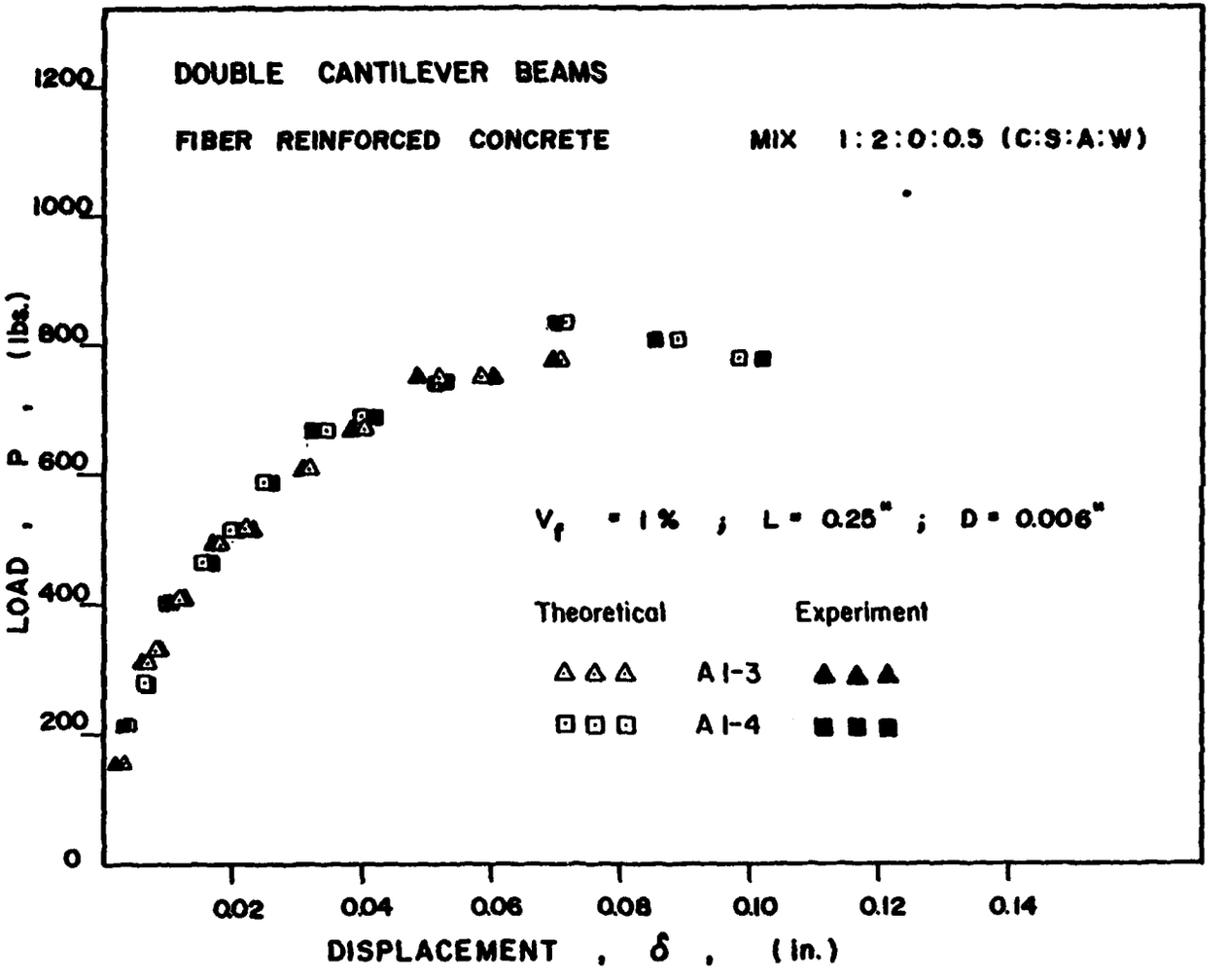

Fig. 17 Comparison of Experimental and Theoretical Permanent Deformation for Fiber Reinforced Concrete DCB

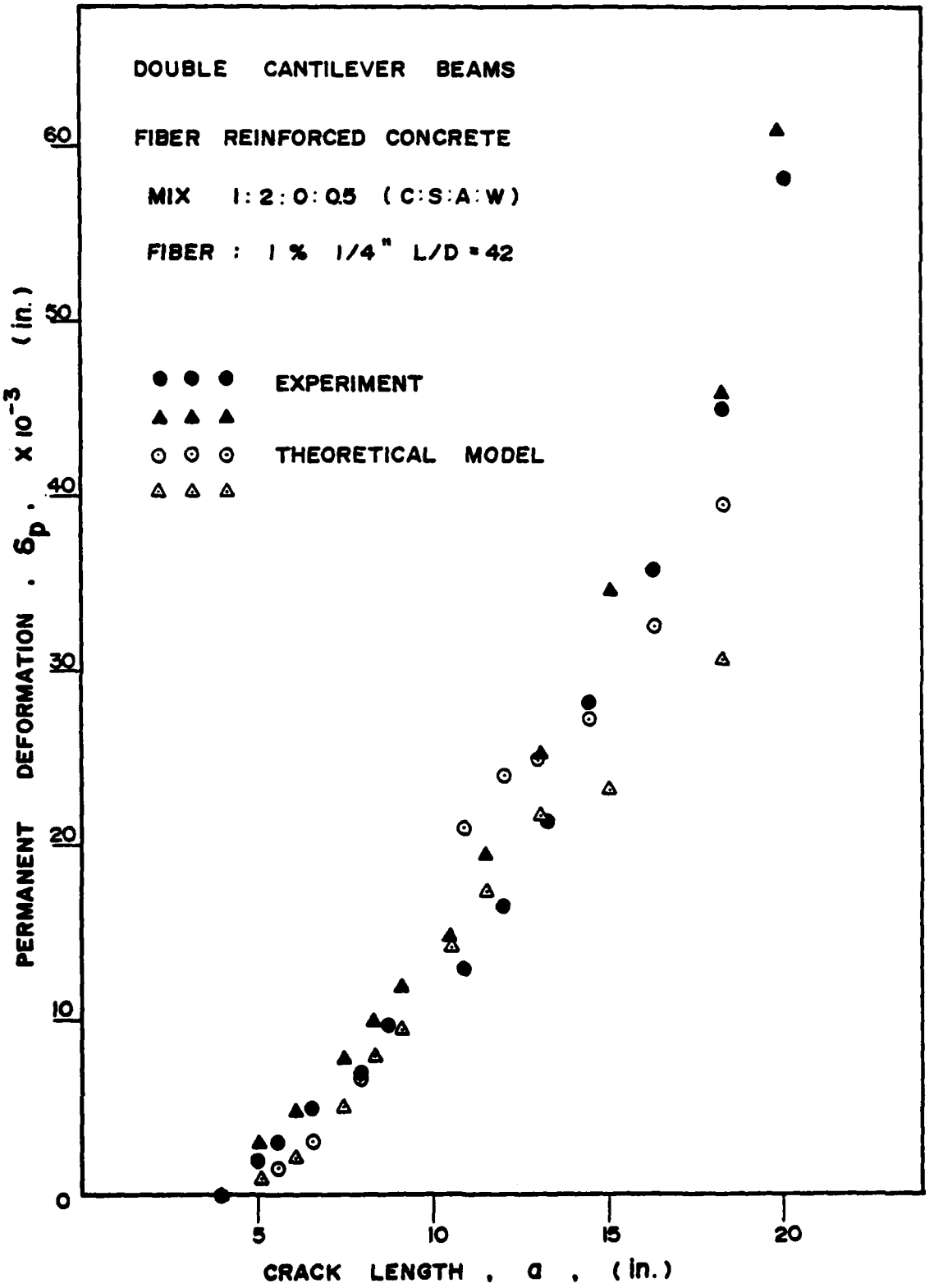

Fig. 18 Comparison of Experimental and Theoretical Permanent Deformation for Fiber Reinforced Concrete - DCB

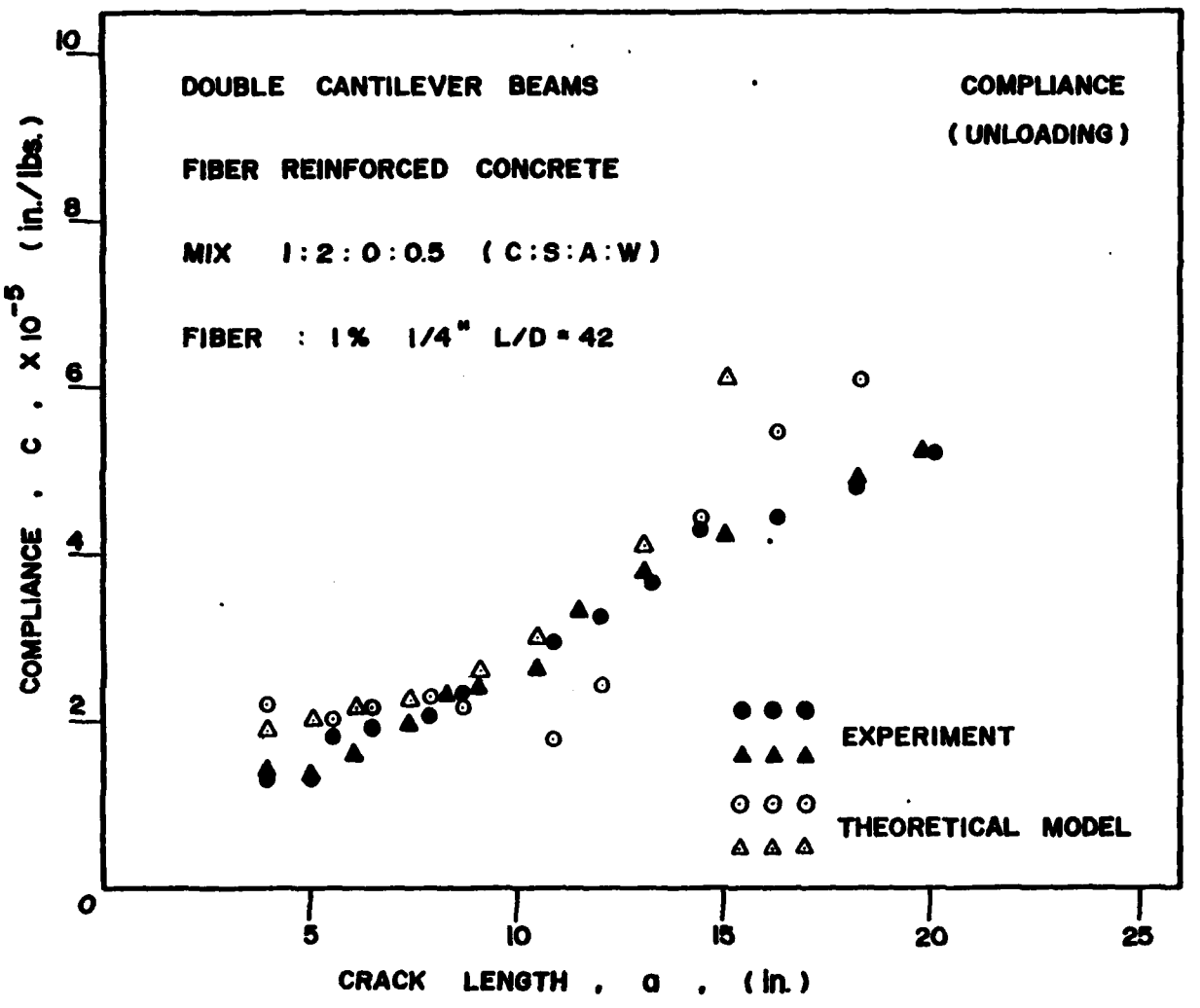

Fig. 19 Experimental and Theoretical Compliances for Fiber

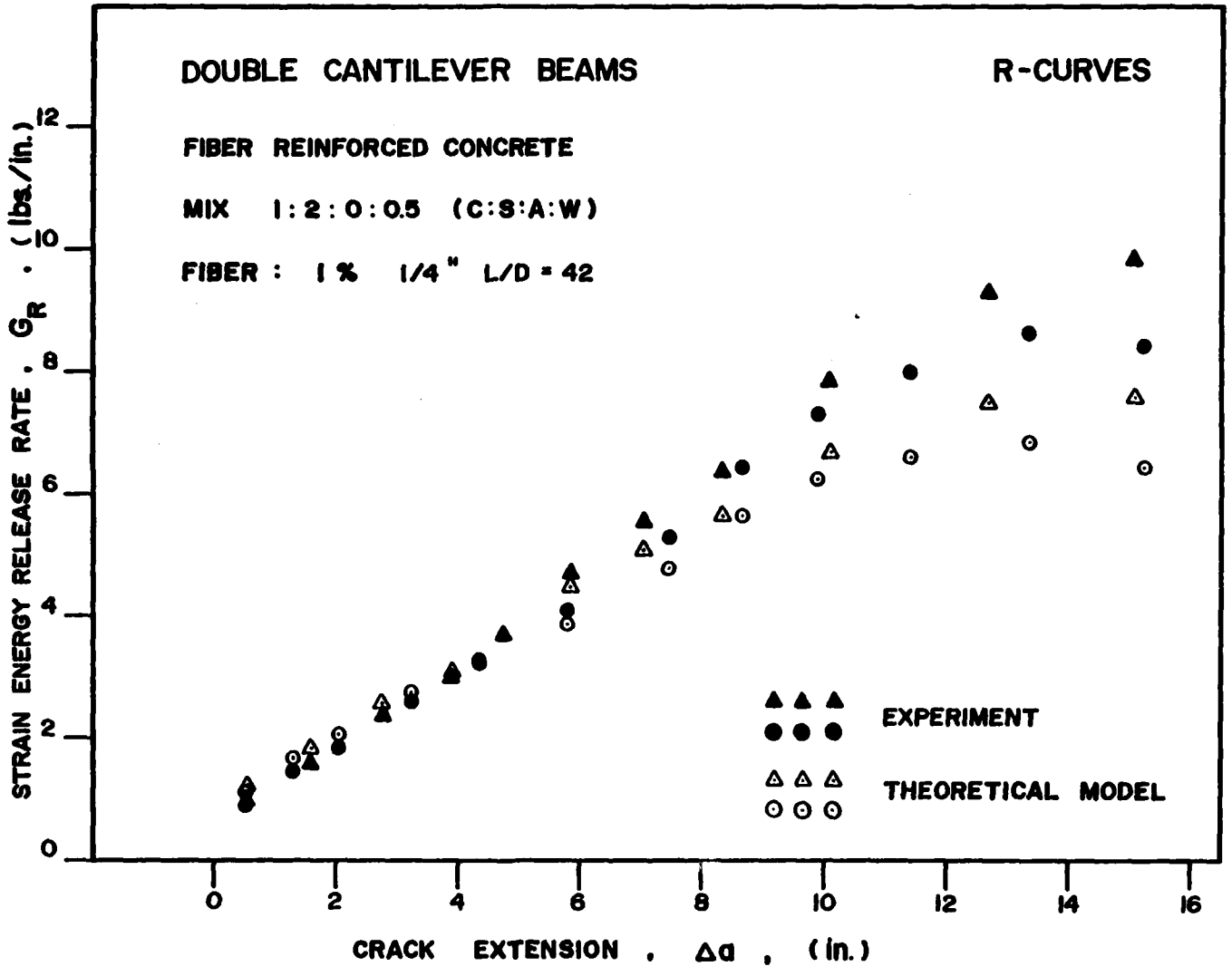

Fig. 20 Experimental and Theoretical G_R - Curves - DCB

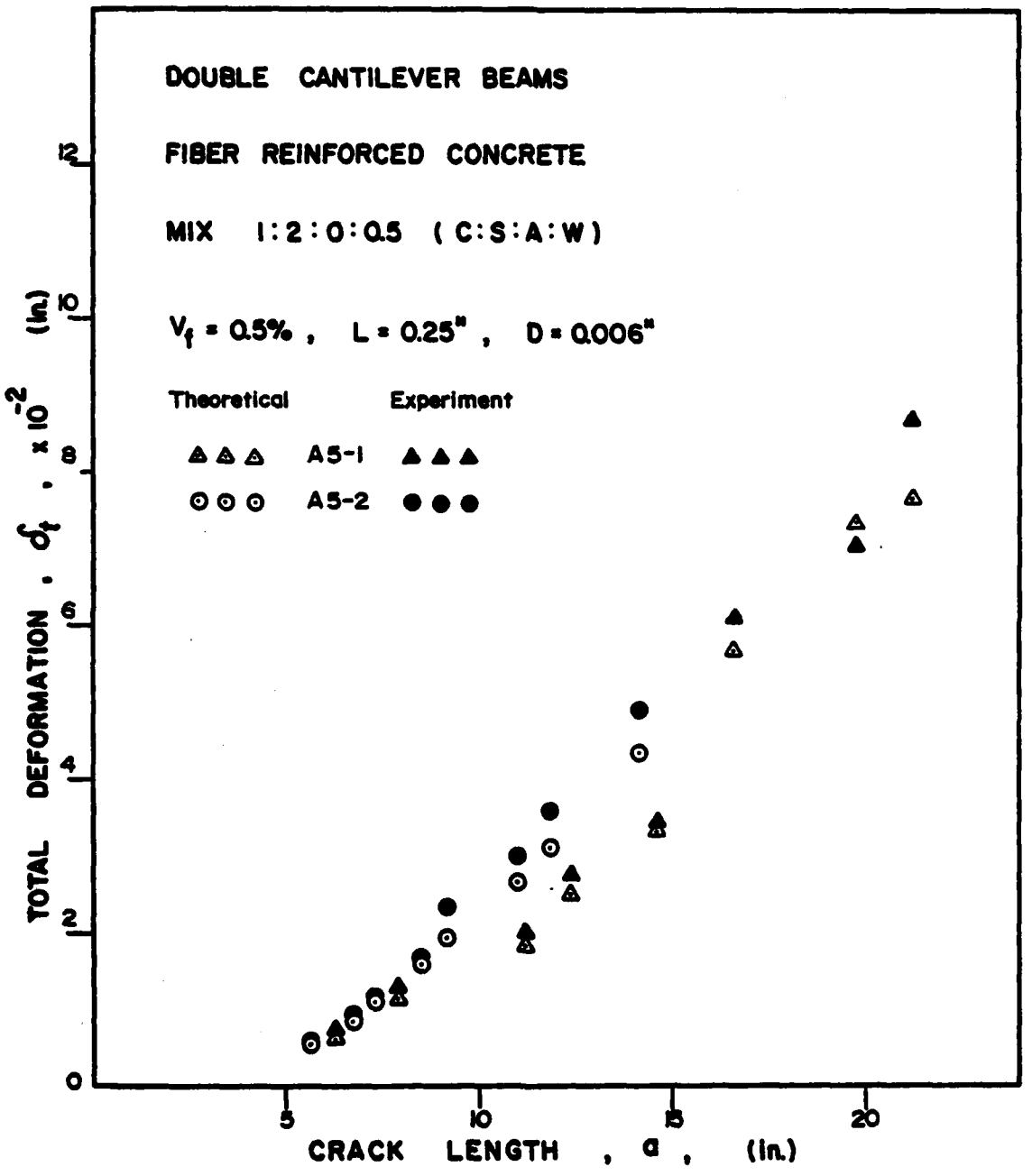

Fig. 21a Experimental and Theoretical Load-Line Deformation and Crack Growth Relationships

V_f = 0.5%, L = 0.25", d = 0.006"

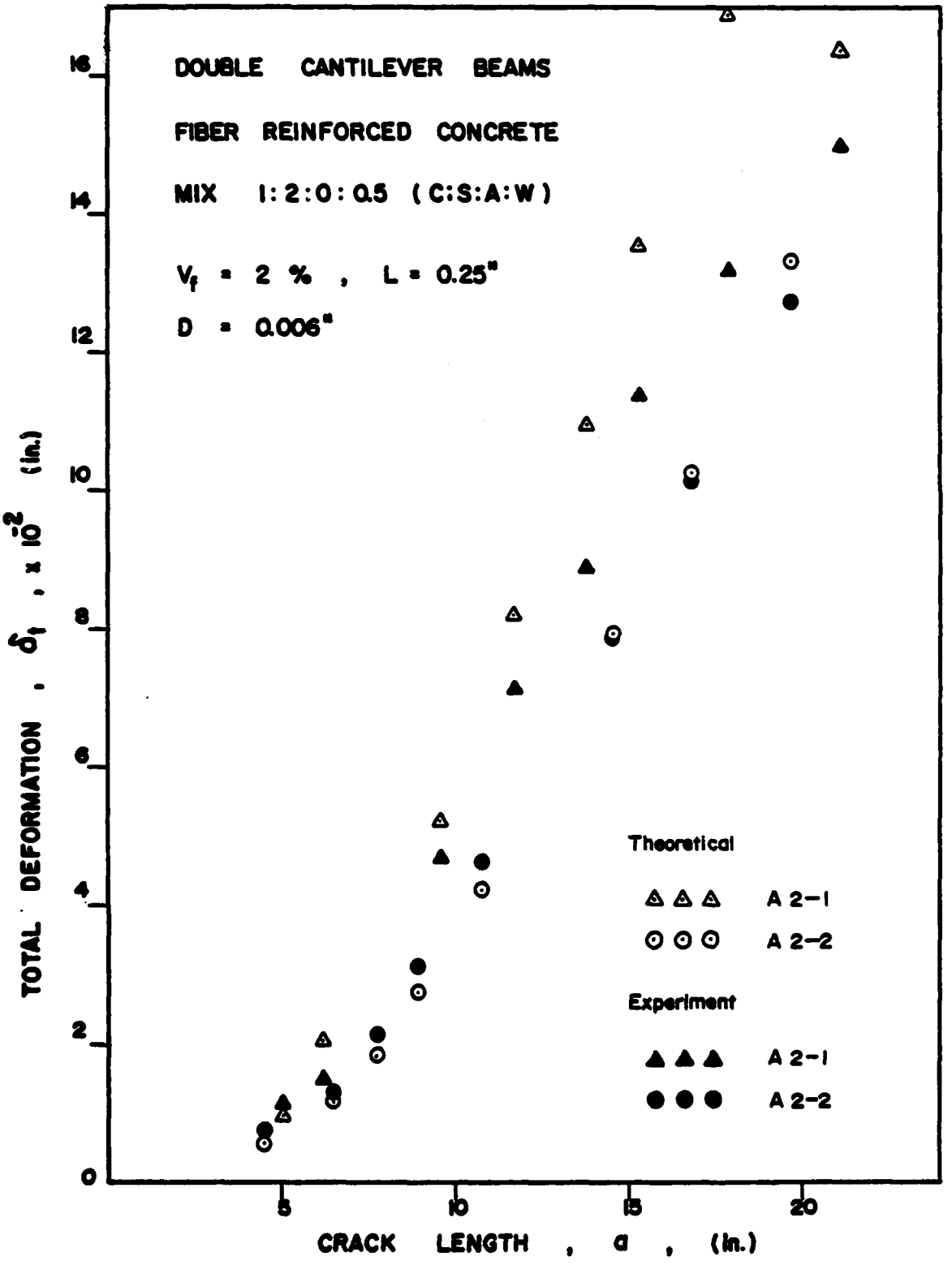

Fig. 21b Experimental and Theoretical Load-Line Deformation and Crack Growth Relationships

F_f = 2%, L = 0.25", d = 0.006"

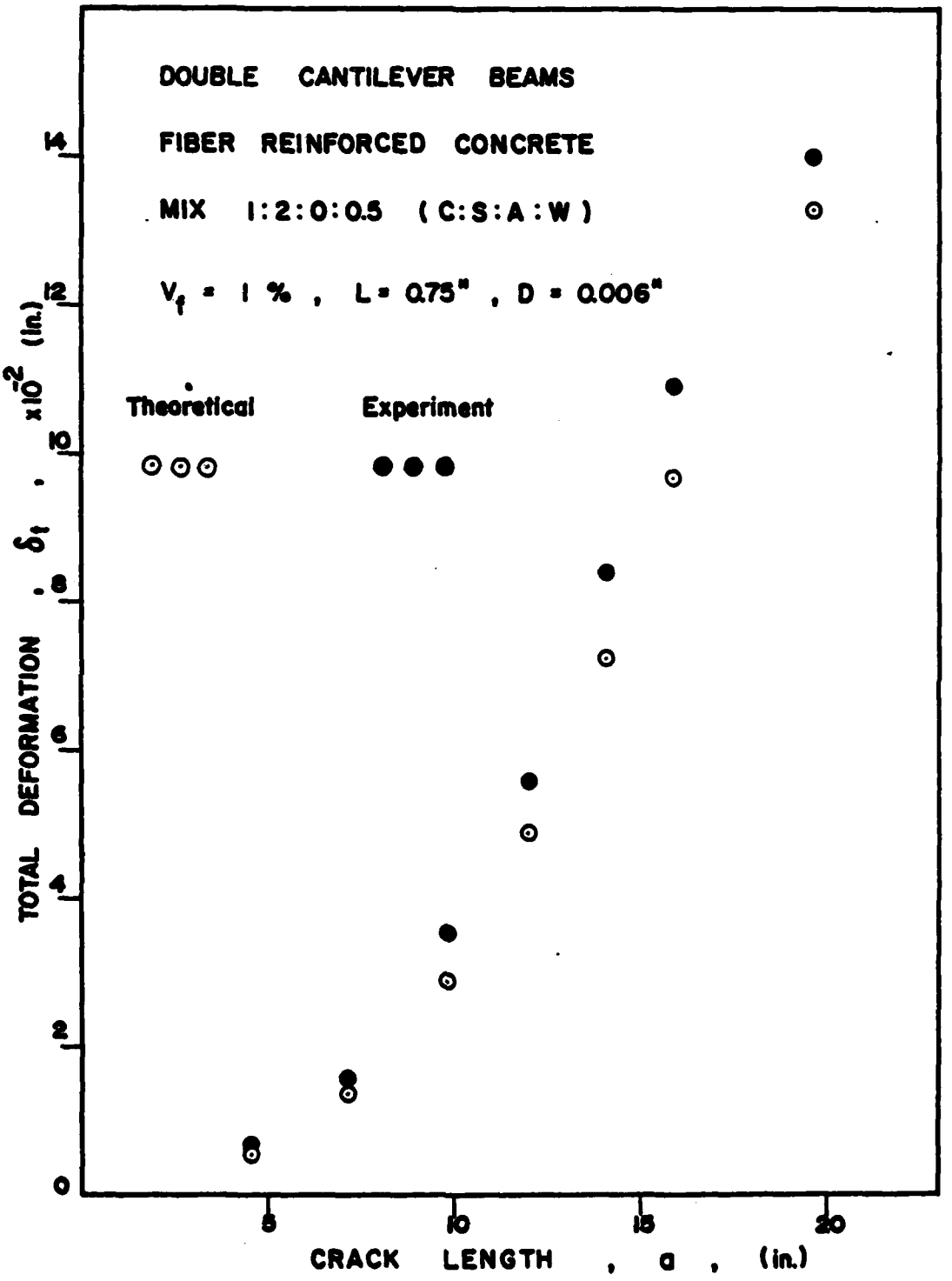

Fig. 21c Experimental and Theoretical Load-Line Deformation and Crack Growth Relationships

V_f = 1%, L = 0.75", d = 0.016"

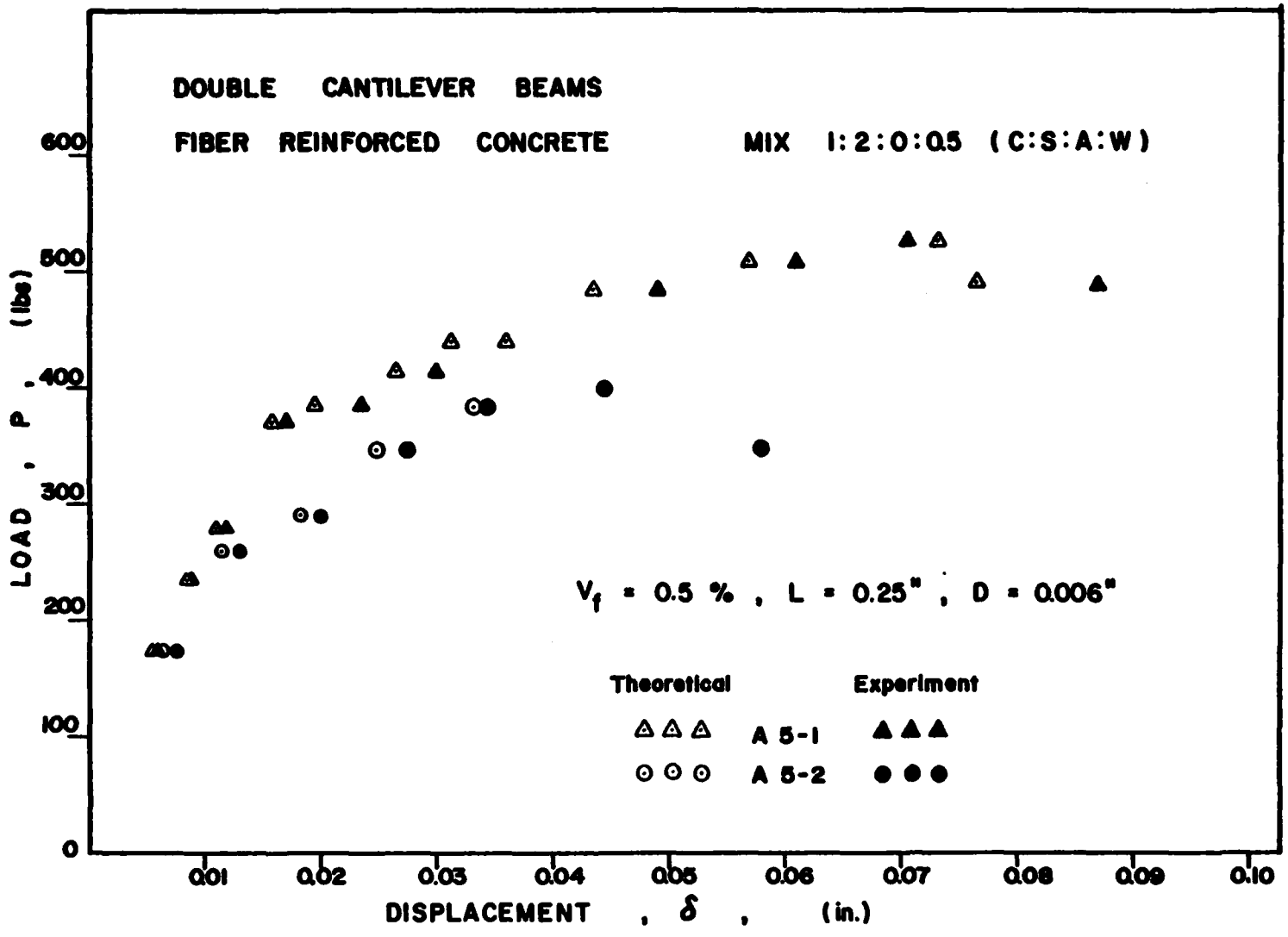

Fig. 22a Experimental and Theoretical Load-Deformation Curves
V_f = 0.5%, L = 0.25", d = 0.006"

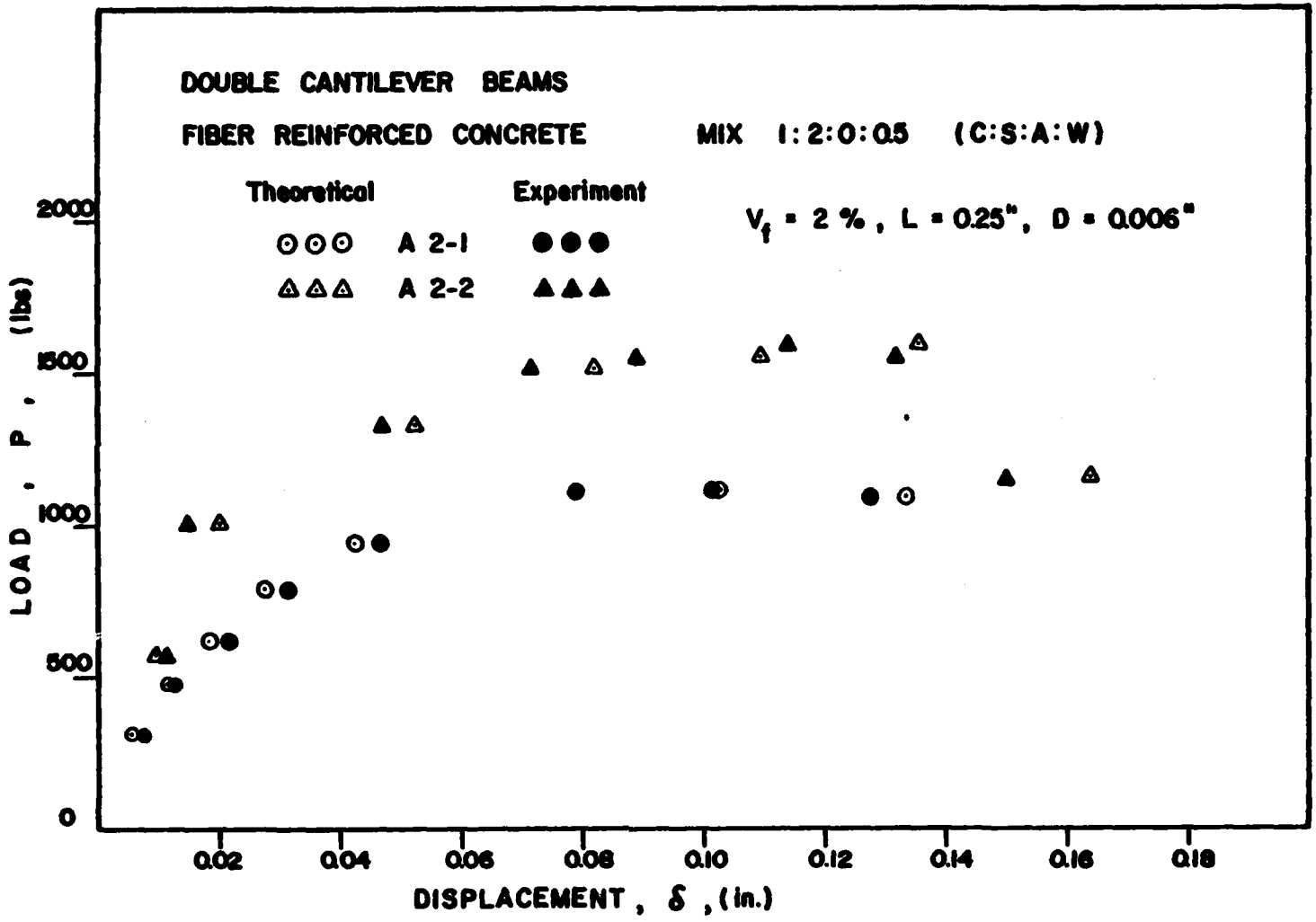

Fig. 22b Experimental and Theoretical Load-Deformation Curves

V_f = 2%, L = 0.25", d = 0.006"

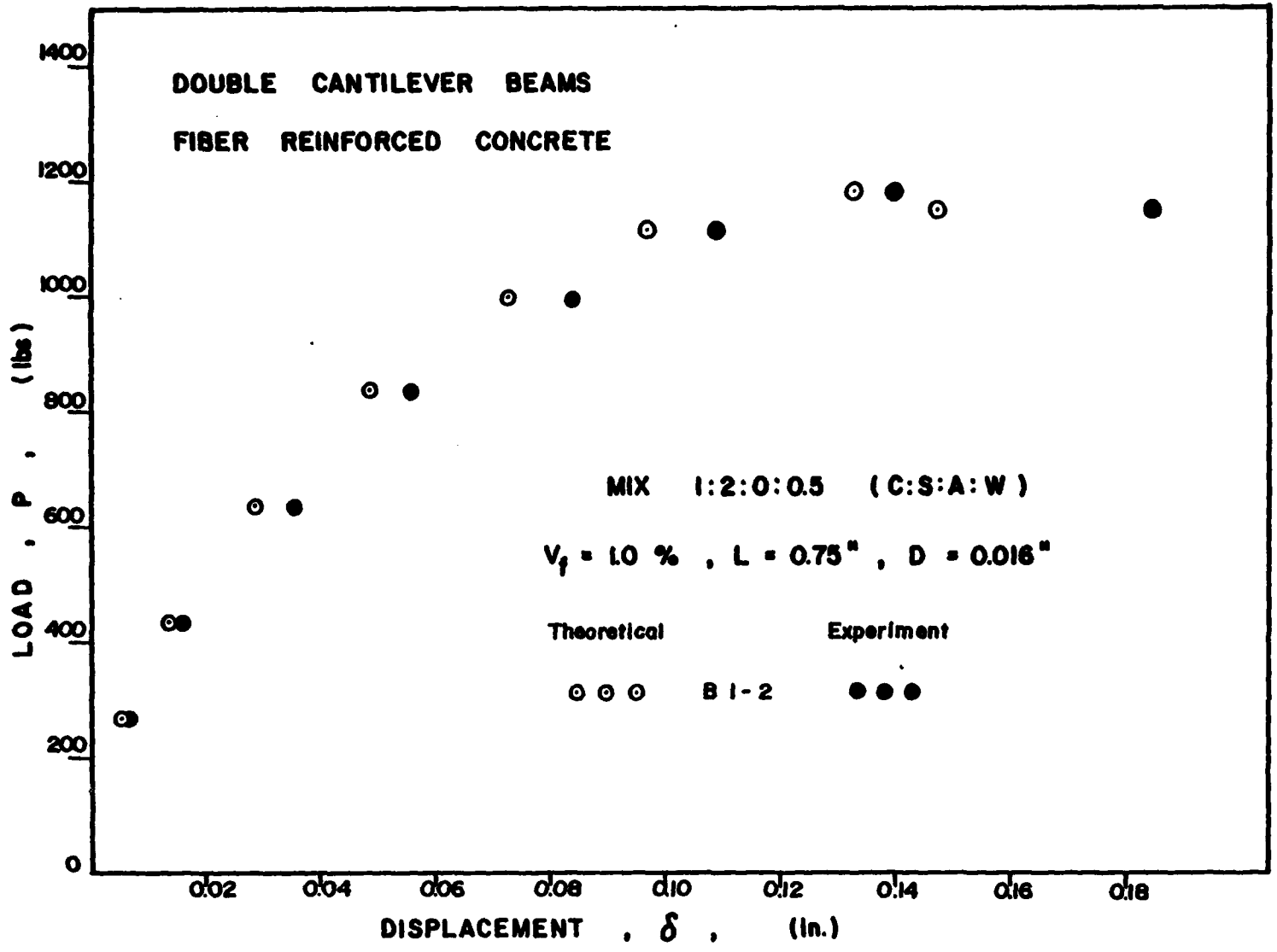

Fig.22c Experimental and Theoretical Load-Deformation Curves

V_f = 1%, L = 0.75", d = 0.016"

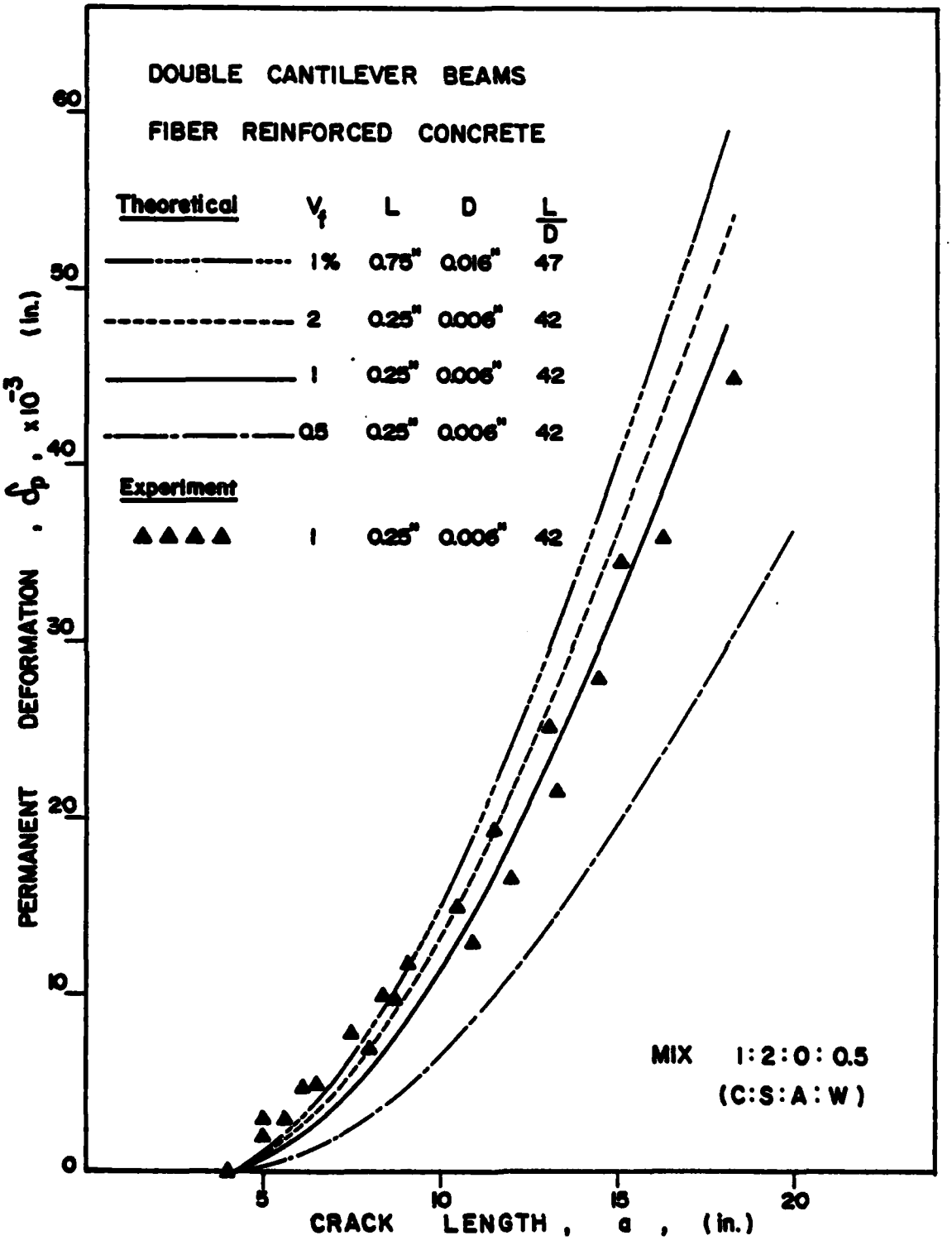

Fig. 23 Comparison of Theoretical Permanent Deformation for Different Fiber Volume Fraction and Aspect Ratio

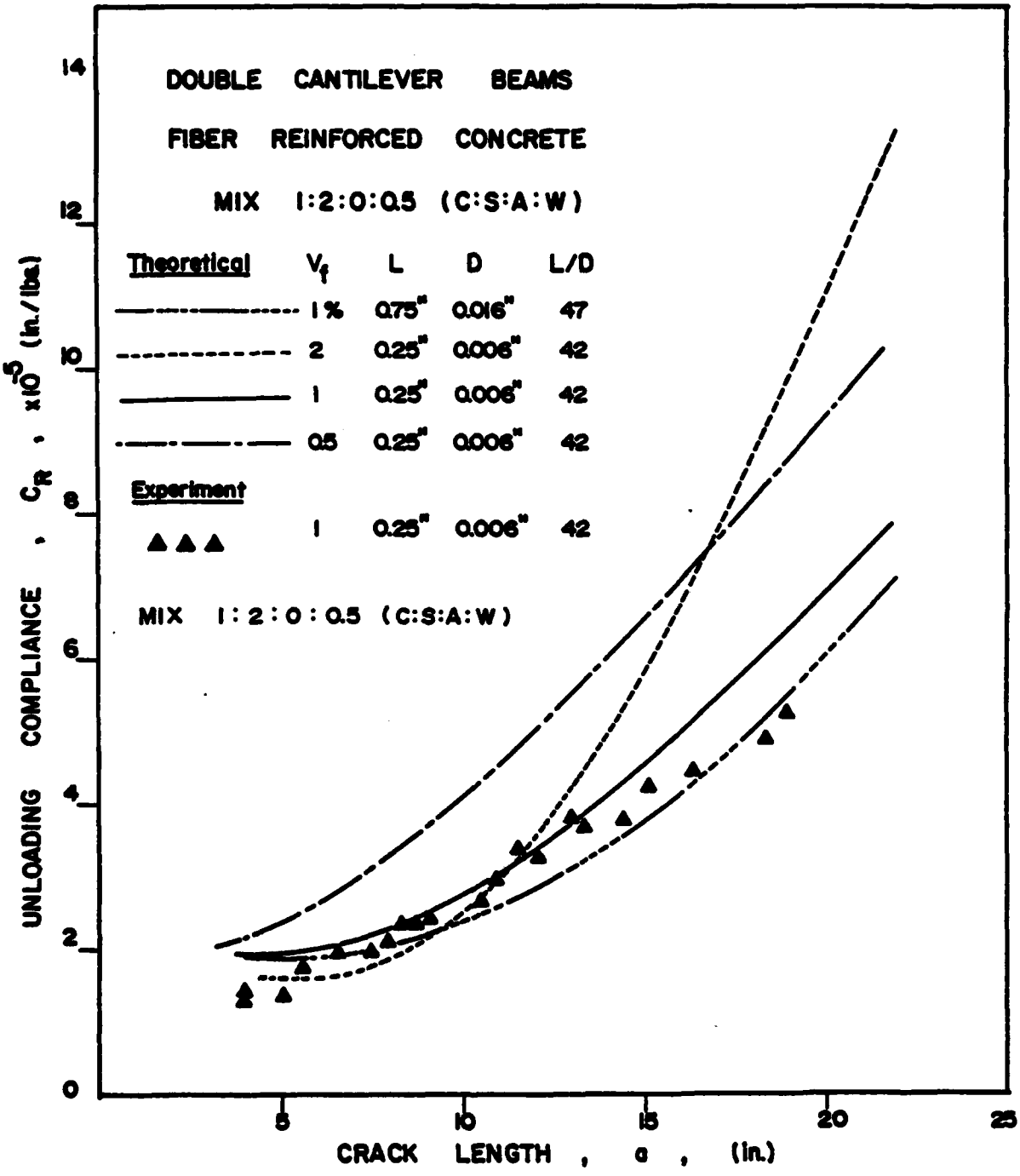

Fig. 24 Comparison of Theoretical Unloading Compliance for Different Fiber Volume Fraction and Aspect Ratio

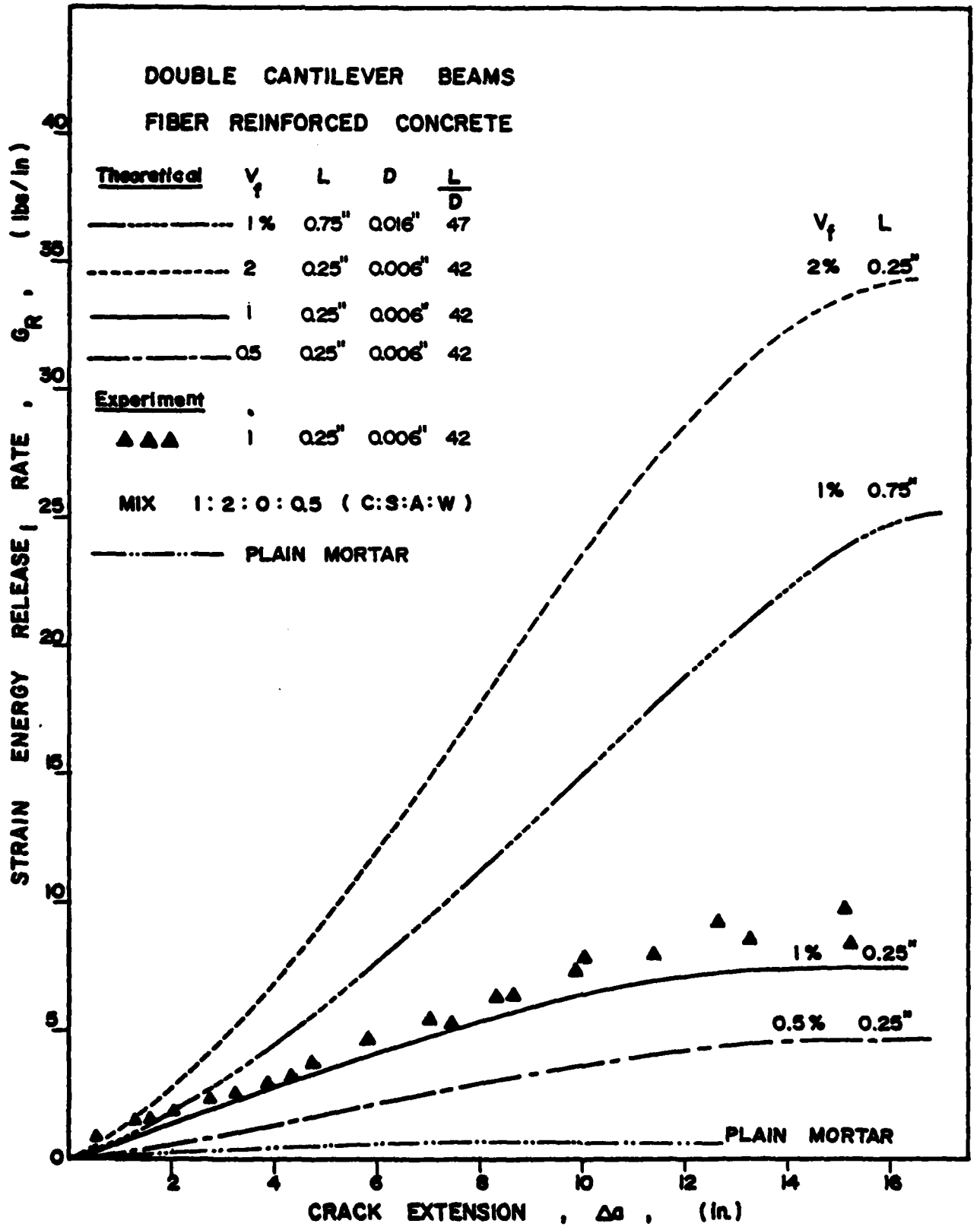

Fig. 25 Comparison of Theoretical Strain Energy Release Rate for Different Fiber Volume Fraction and Aspect Ratio

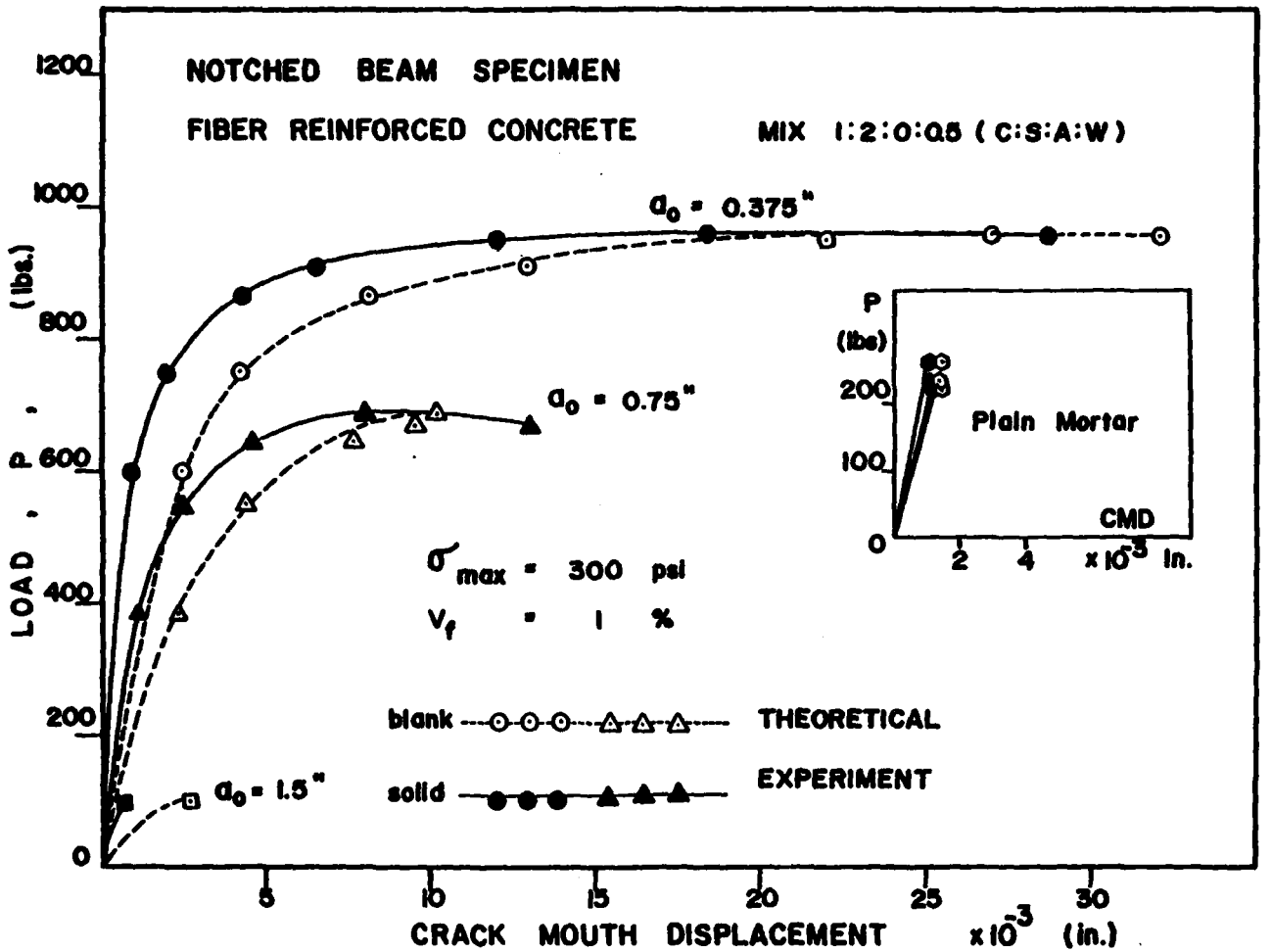

Fig. 26 Comparison of Experimental and Theoretical Load-Crack Mouth Displacement in Notched Beam Specimens

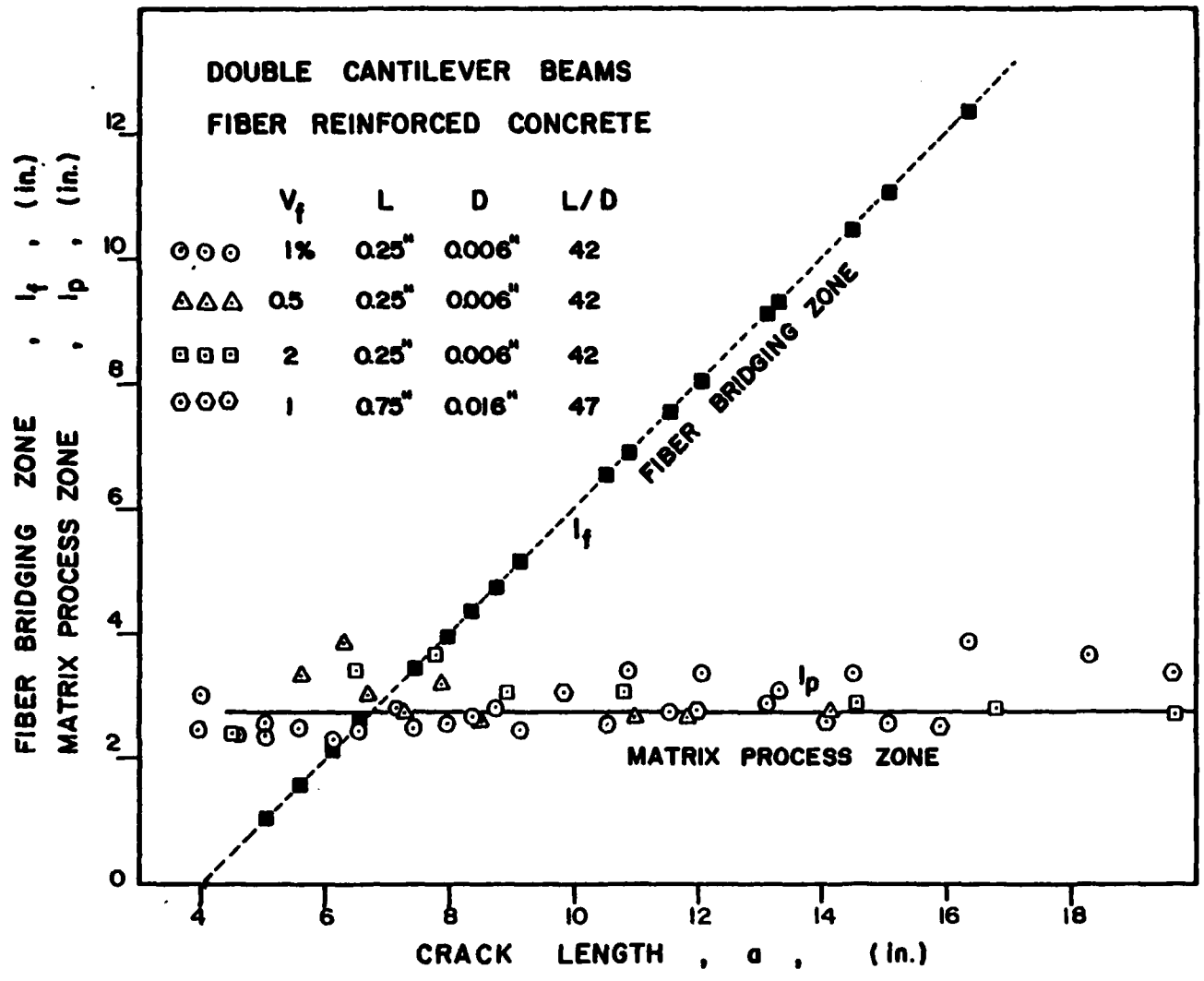

Fig. 27 Matrix Process Zone and Fiber Bridging Zone in Fiber Reinforced Concrete - DCB Specimens

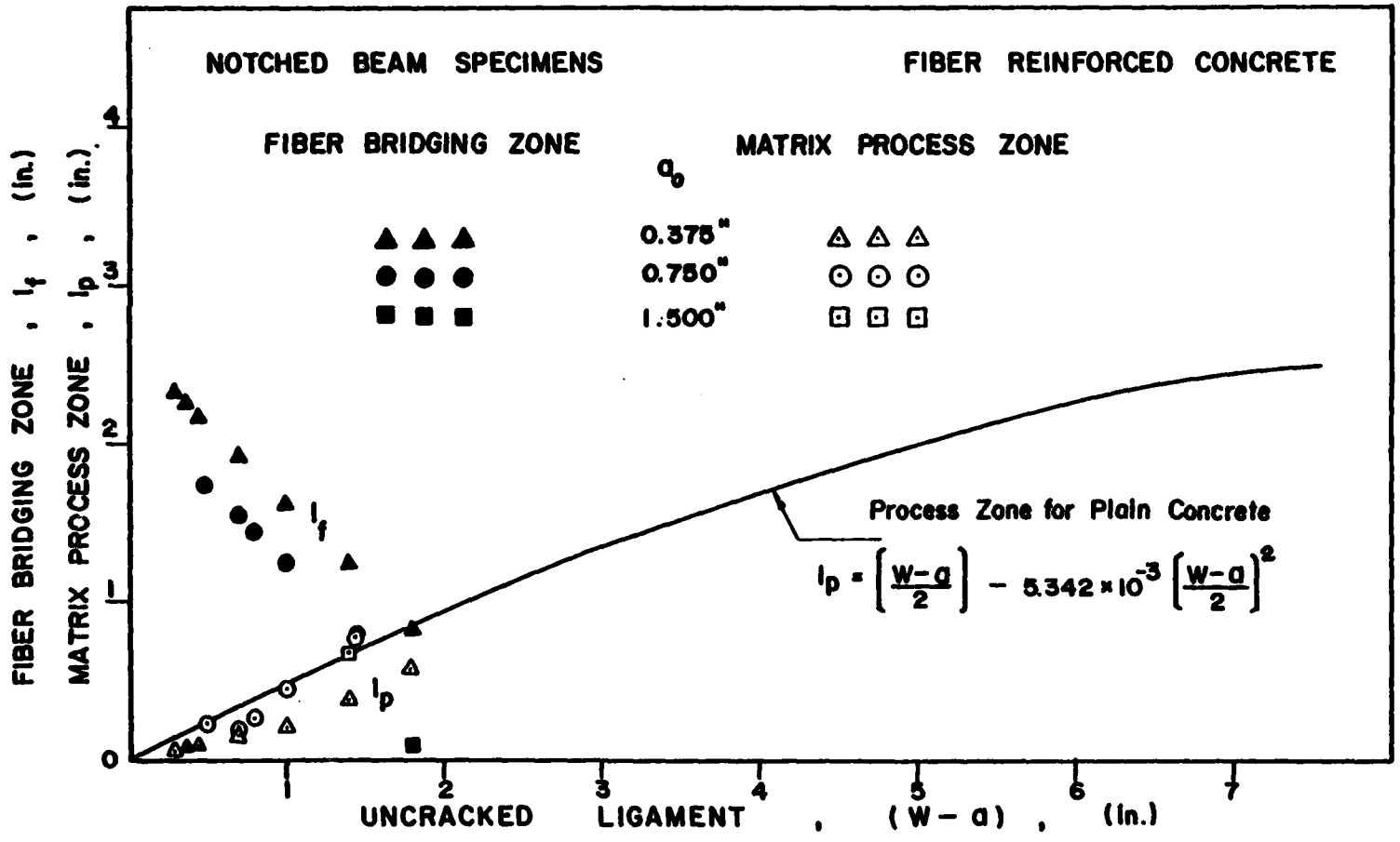

Fig. 28 Matrix Process Zone and Fiber Bridging Zone in Fiber Reinforced Concrete - Notched Beam Specimens

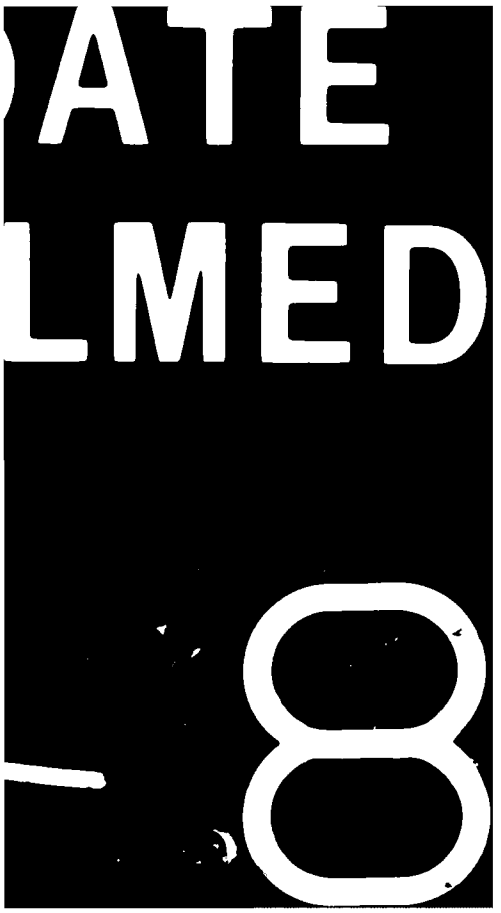
ATE
LMED
8